Particle Simulation of Various Gold Nanoantennas in Laser Irradiated Matter for Fusion Production

István Papp, Konstantin Zhukovsky, et al.
(part of NAPLIFE Collaboration)

Symposium on Particles & Plasmas, Budapest

June 12, 2024

Nanoplasmonic Laser Fusion Research Laboratory

Kőszeg, September 14, 2019 - Int. Workshop on Collectivity
First meeting on the NAPLIFE project (12 people)

Introduction

Thermo-nuclear Fusion

- ηE_f is the usable energy
- The loss is $(1-\eta)(E_0+E_b)$
- $E_0 = 3nkT$, $E_b = bn^2\tau\sqrt{T}$ (thermal bremsstralung)
- Giving the gain factor: $Q = \frac{\eta\epsilon n\tau v\sigma}{4(1-\eta)(3kT+bn\tau\sqrt{T})}$
- Q must be $Q > 1$ for energy production
- This also means $n\tau > \frac{3kT(1-\eta)}{\frac{1}{4}\epsilon\eta\langle v\sigma\rangle - b(1-\eta)\sqrt{T}} \rightarrow$ LC

Lawson criterion

Fulfilling the Lawson criterion

- Magnetically confined plasmas: increase confinement time
- Inertial confinement fusion: increase density of fusion plasma

Article

https://doi.org/10.1038/s41467-023-36655-1

First measurements of $p^{11}B$ fusion in a magnetically confined plasma

Received: 4 November 2022

Accepted: 10 February 2023

Published online: 21 February 2023

Check for updates

R. M. Magee[1] ✉, K. Ogawa[2], T. Tajima[1,3], I. Allfrey[1], H. Gota[1], P. McCarroll[1], S. Ohdachi[2], M. Isobe[2], S. Kamio[1,3], V. Klumper[1,3], H. Nuga[2], M. Shoji[2], S. Ziaei[1], M. W. Binderbauer[1] & M. Osakabe[2]

Proton-boron ($p^{11}B$) fusion is an attractive potential energy source but technically challenging to implement. Developing techniques to realize its potential requires first developing the experimental capability to produce $p^{11}B$ fusion in the magnetically-confined, thermonuclear plasma environment. Here we report clear experimental measurements supported by simulation of $p^{11}B$ fusion with high-energy neutral beams and boron powder injection in a high-temperature fusion plasma (the Large Helical Device) that have resulted in diagnostically significant levels of alpha particle emission. The injection of boron powder into the plasma edge results in boron accumulation in the core. Three 2 MW, 160 kV hydrogen neutral beam injectors create a large population of well-confined, high -energy protons to react with the boron plasma. The fusion products, MeV alpha particles, are measured with a custom designed particle detector which gives a fusion rate in very good relative agreement with calculations of the global rate. This is the first such realization of $p^{11}B$ fusion in a magnetically confined plasma.

The proton–boron fusion reaction ($p^{11}B$),

$$p(^{11}B, \alpha)\alpha\alpha + 8.7\,\text{MeV} \quad (1)$$

While the challenges of producing the fusion core are greater for $p^{11}B$ than DT, the engineering of the reactor will be far simpler. The enormous fluence of 14 MeV neutrons from a DT reactor plasma

News on fusion

Quasi-IsoDynamic Stellarator

first light

HB11 ENERGY
LASER BORON FUSION

National Ignition Facility LLNL first year of sooting

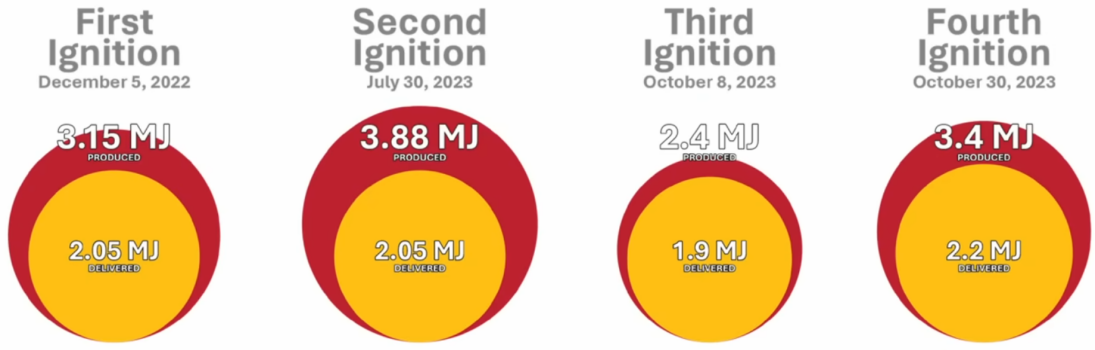

LLNL has achieved fusion ignition on NIF four times to date. Credit: Brian Chavez

FUNDING FOR FUSION COMPANIES

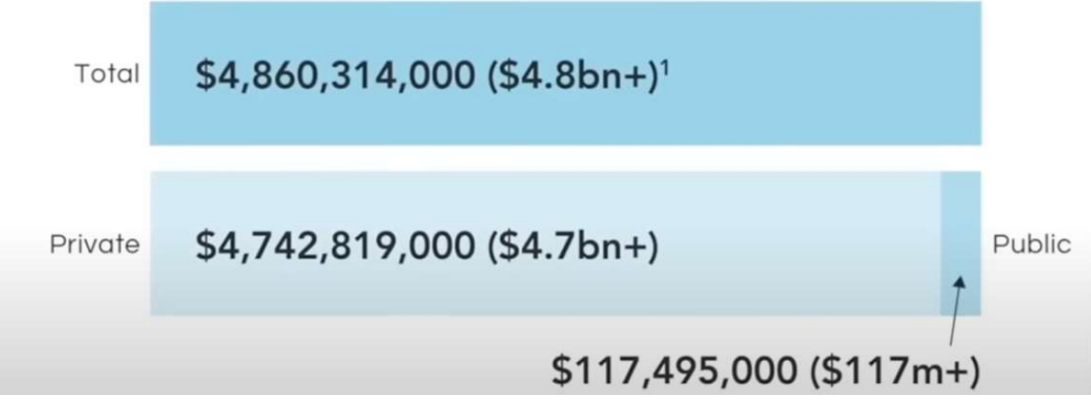

Tri alpha Energy (TAE) Technologies	1998	USA	$1.3B	Magnetic Confinement
Helion Energy	2013	USA	$577.8M	Magneto-inertial fusion
General Fusion	2002	Canada	$437M	Magneto-inertial fusion
Shine Technologies	2005	USA	$414M	Magnetic Confinement
Zap Energy	2017	USA	$207.8M	Magneto-inertial fusion
Tokamak Energy	2009	UK	$156.8M	Magnetic Confinement
General Atomic	1955	USA	$113 M	Magnetic Confinement
First Light Fusion	2011	UK	$107M	Inertial Confinement
Energy Singularity Fusion Power Technology	2021	China	$112M	Magnetic Confinement
Kyoto Fusioneering	2019	Japan	$82M	Magnetic Confinement
Focused Energy	2021	USA	$79M	Inertial Confinement
Marvel Fusion	2019	Germany	$65M	Inertial Confinement
Avalanche Energy	2018	USA	$51.6M	Inertial Confinement
Type One Energy	2019	USA	$29M	Magnetic Confinement
HB11	2019	Australia	$22M	Inertial Confinement
NT-Tao	2016	Israel	$22M	Magnetic Confinement
Helical Fusion	2013	Japan	$19.4M	Magnetic Confinement
Fuse Energy Technology	2019	USA	$18M	Magneto-inertial fusion
Renaissance Fusion	2019	France	$16.4M	Magnetic Confinement
Ex-Fusion	2021	Japan	$13.5M	Inertial Confinement
Realta Fusion	2021	USA	$12M	Magnetic Confinement
Lawrenceville Plasma Physics	2003	USA	$10M	Inertial Confinement
Novatron	2019	Sweden	$8.55M	Magnetic Confinement
Proxima Fusion	2023	Germany	$8M	Magnetic Confinement
Gauss Fusion	2021	Germany	$8M	Magnetic Confinement
Nk Labs	2008	USA	$2.5M	Muon-catalyzed fusion
Deutelio	2022	Italy	$534K	Magnetic Confinement
Blue Laser Fusion	2022	USA	$500K	Inertial confinement
Crossfield Fusion	2019	UK	$500K	Magnetic Confinement
Electric Fusion Systems	2020	USA	$400K	Magnetic Confinement
NearStar Fusion	2021	USA	$390K	Magneto-inertial fusion

Direct vs Indirect drive

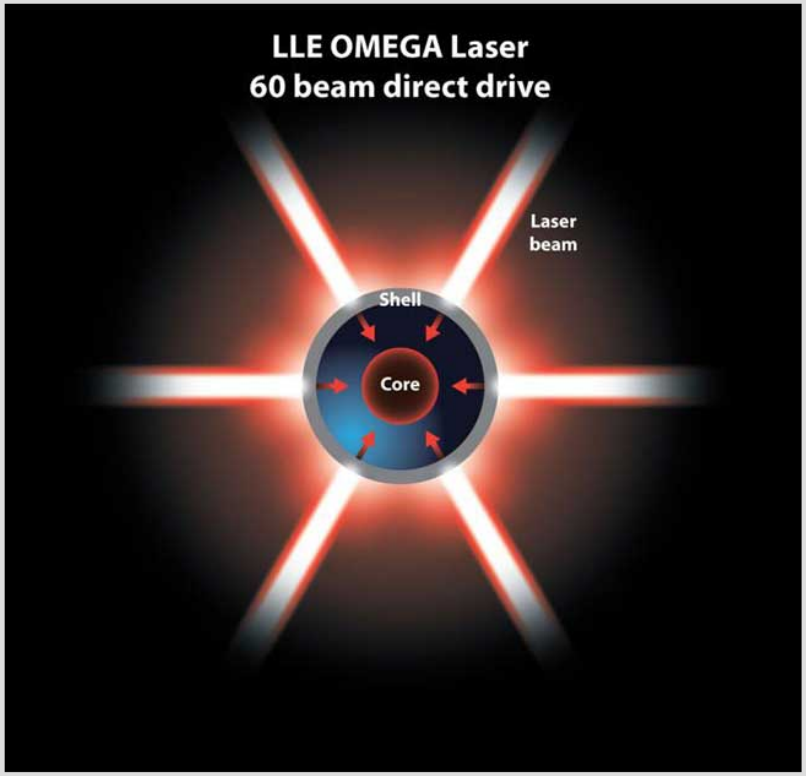

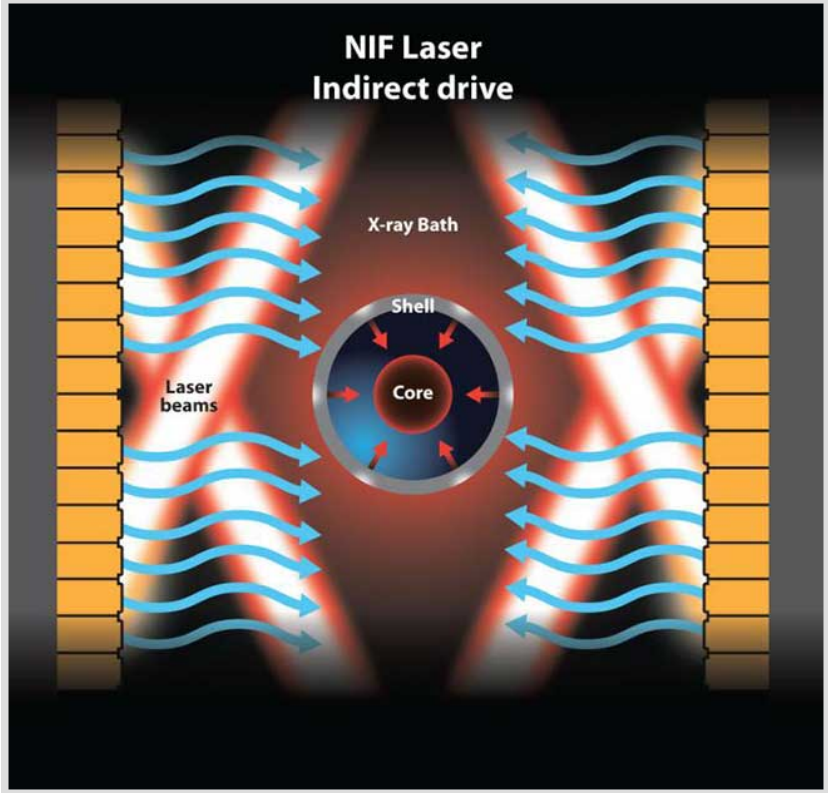

PHOTONICS MEDIA photonics.com

Hohlraum

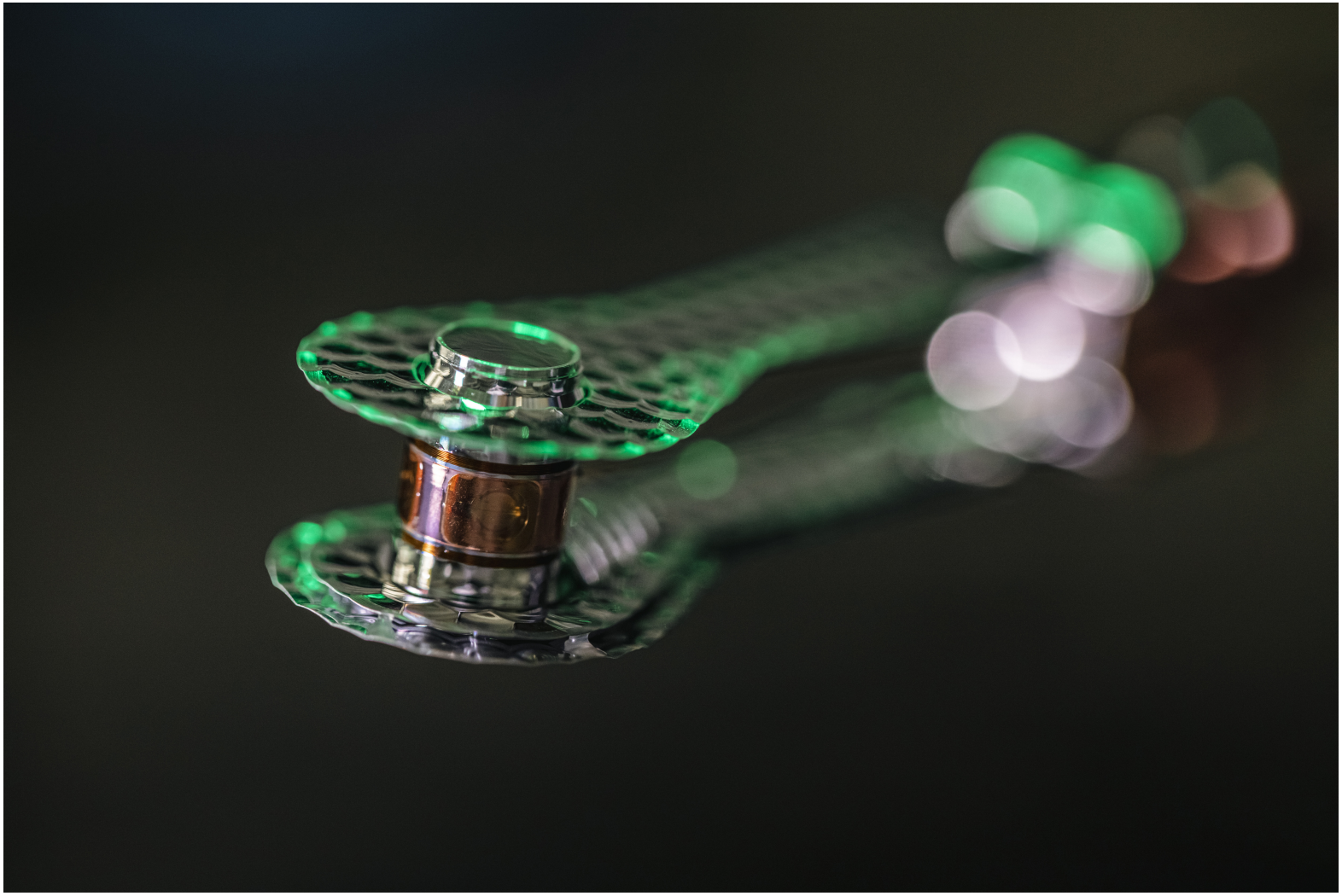

Hohlraum 2014

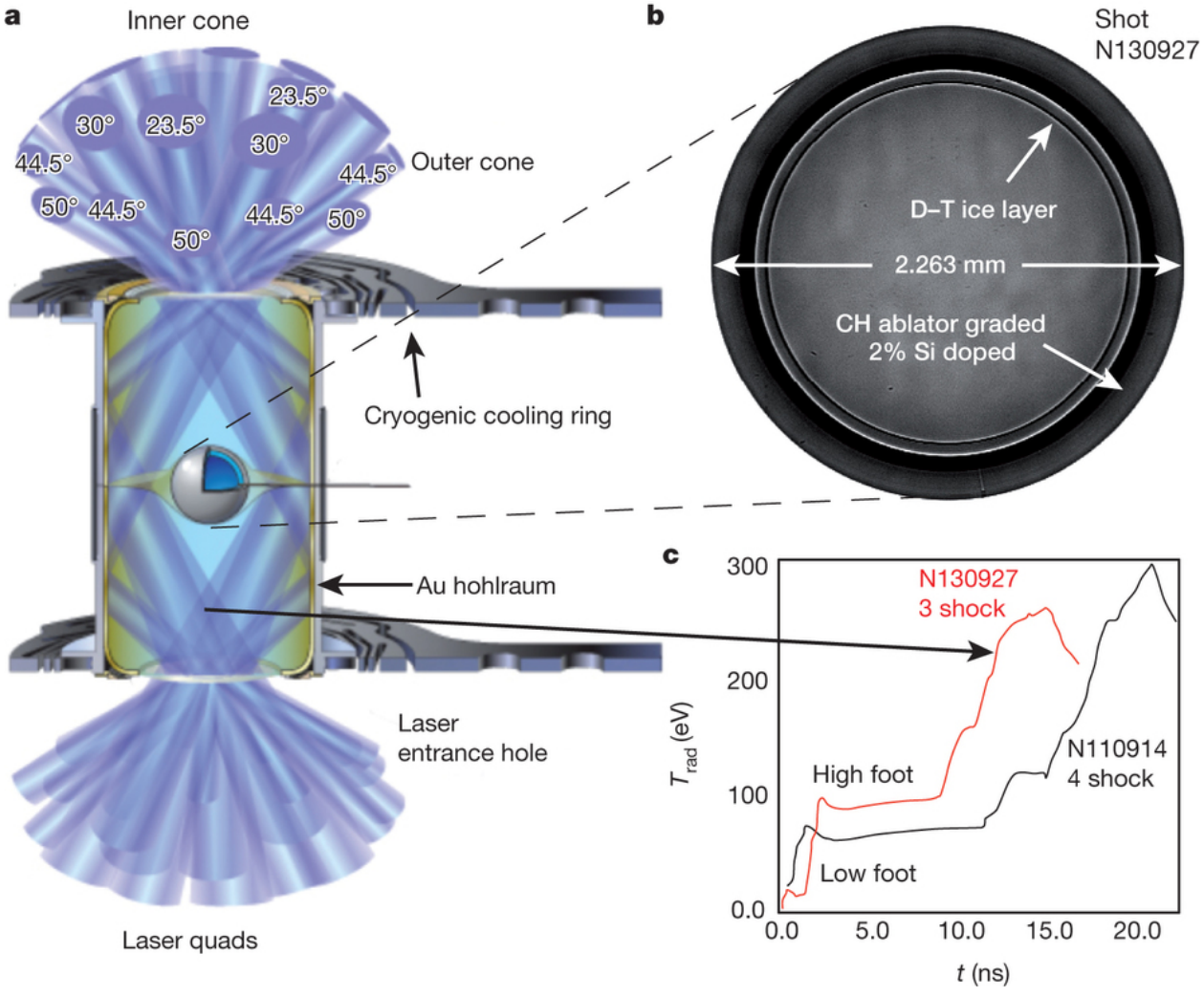

[O.A. Hurricane et al., Nature, 506, 343 (2014)]

Hohlraum 2022

Fig. 1: Schematic of the indirect-drive inertial confinement approach to fusion.

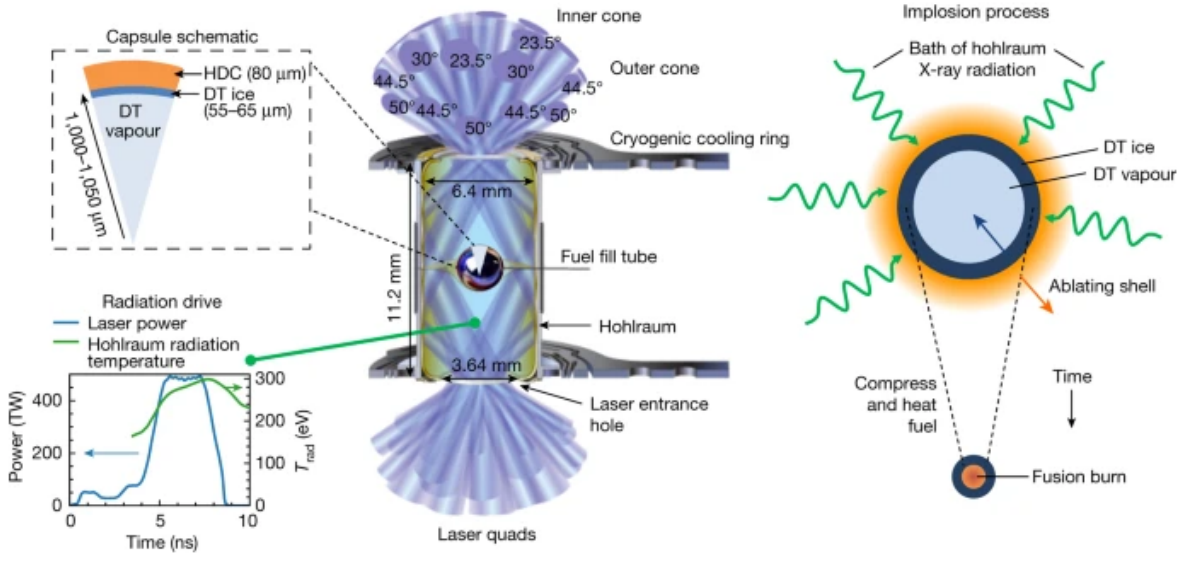

Centre, A typical indirect-drive target configuration with key engineering elements labelled. Laser beams (blue) enter the hohlraum through laser entrance holes at various angles. Top left, A schematic pie diagram showing the radial distribution and dimensions of materials in diamond (high-density carbon, HDC) ablator implosions. Bottom left, The temporal laser power pulse-shape (blue) and associated hohlraum radiation temperature (green). Right, At the centre of the hohlraum, the capsule

[A.B, Zylstra, O.A. Hurricane et al., Nature, 601, 542-548 (2022)]

Rayleigh-Taylor instabilities

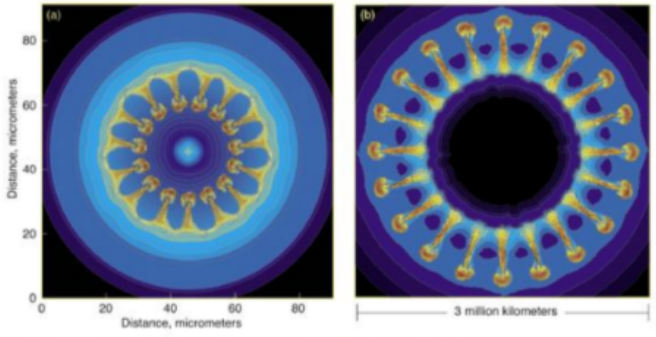

Striking similarities exist between hydrodynamic instabilities in (a) inertial confinement fusion capsule implosions and (b) core-collapse supernova explosions. [Image (a) is from Sakagami and Nishihara, *Physics of Fluids B* **2**, 2715 (1990); image (b) is from Hachisu et al., *Astrophysical Journal* **368**, L27 (1991).]

Energy must be delivered as sysmmetric as possible!

Different levels of corrugation of the shell surfaces :

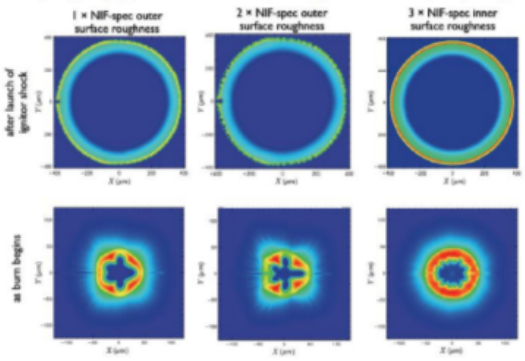

Left: same roughness of inner and outer surface as specified for the NIF target
Center: outer surface roughness is twice the NIF level
Right: DT inner surface roughness three times larger than NIF specifications

[S. Atzeni et al., Nucl. Fusion 54, 054008 (2014).] 25

Latest (January 2023) news 3.15MJ kinetic energy at NIF with burning time of 89-137 ps(?)

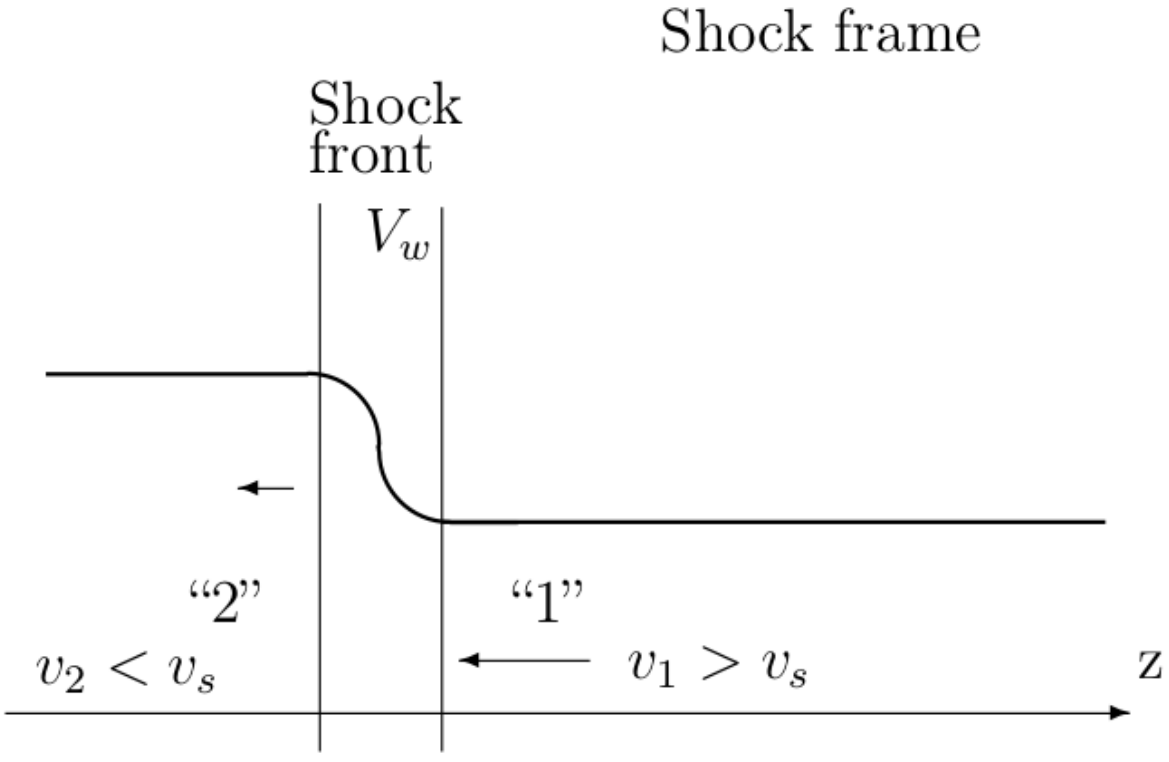

[Csernai, L.P. (1987). Detonation on a time-like front for relativistic systems. Zh. Eksp. Teor. Fiz. 92, 379-386.]

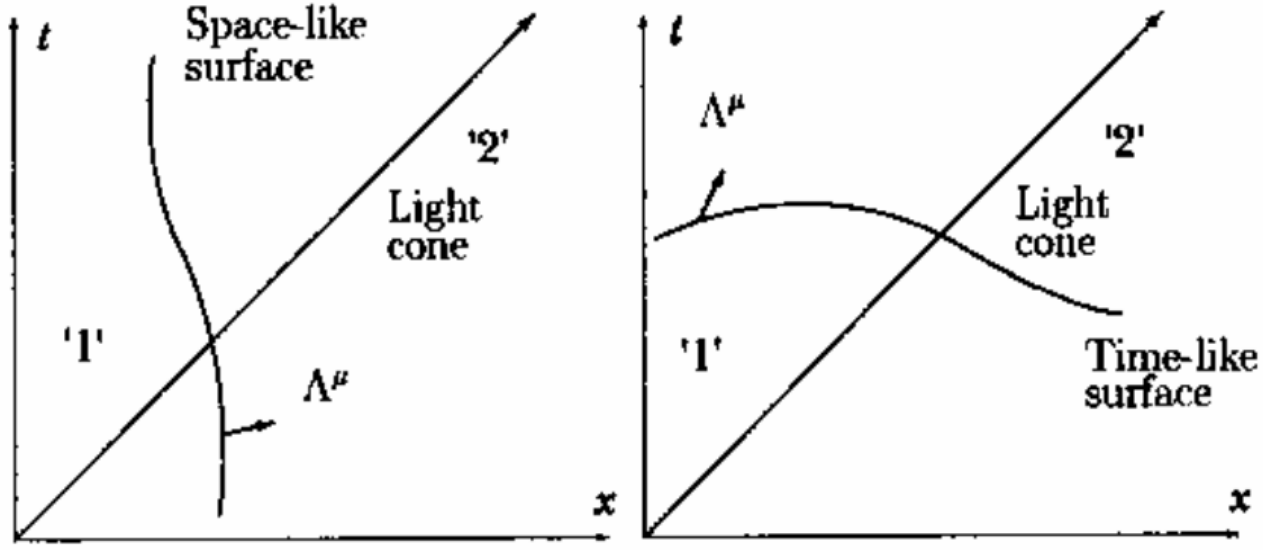

Figure 5.9: Space-like (a) and time-like (b) surfaces of discontinuity

[Csernai, L.P. (1987). Detonation on a time-like front for relativistic systems. Zh. Eksp. Teor. Fiz. 92, 379-386.]

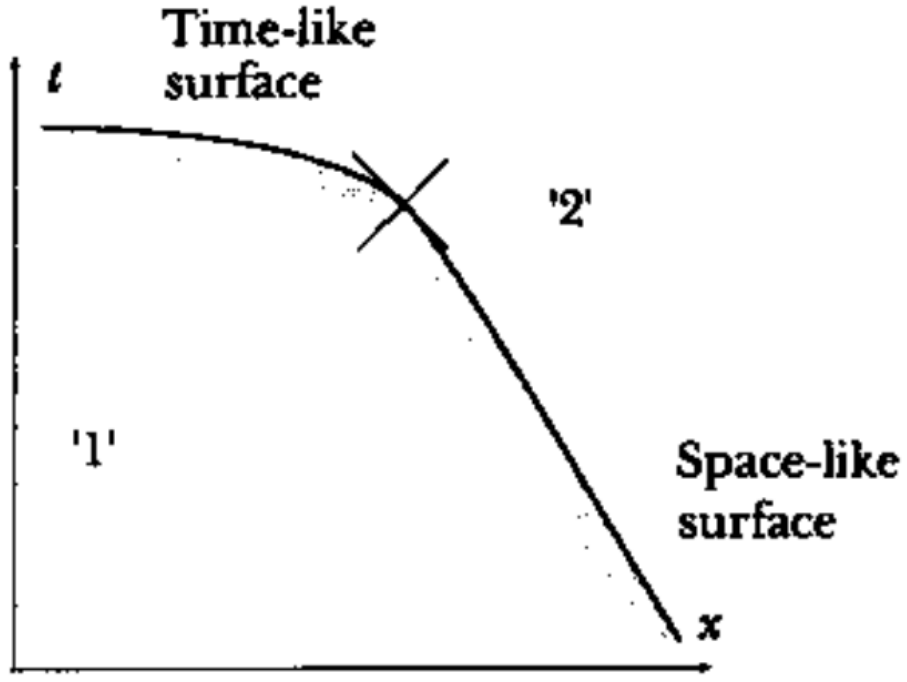

Figure 5.10: Smooth change from spacelike to timelike detonation

[Csernai, L.P. (1987). Detonation on a time-like front for relativistic systems. Zh. Eksp. Teor. Fiz. 92, 379-386.]

Constant absorptivity

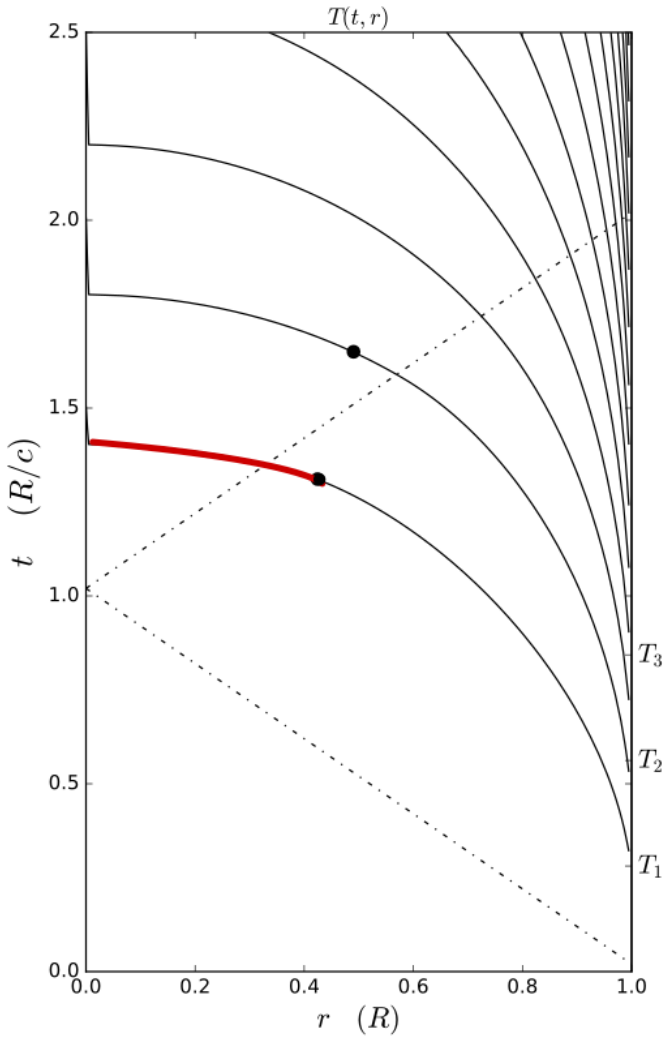

[L.P. Csernai & D.D. Strottman, Laser and Particle Beams 33, 279 (2015)]

$\alpha_{k_{middle}} = \alpha_{k_{edge}}$

Simultaneous volume ignition is only up to 12%

Changing absorptivity

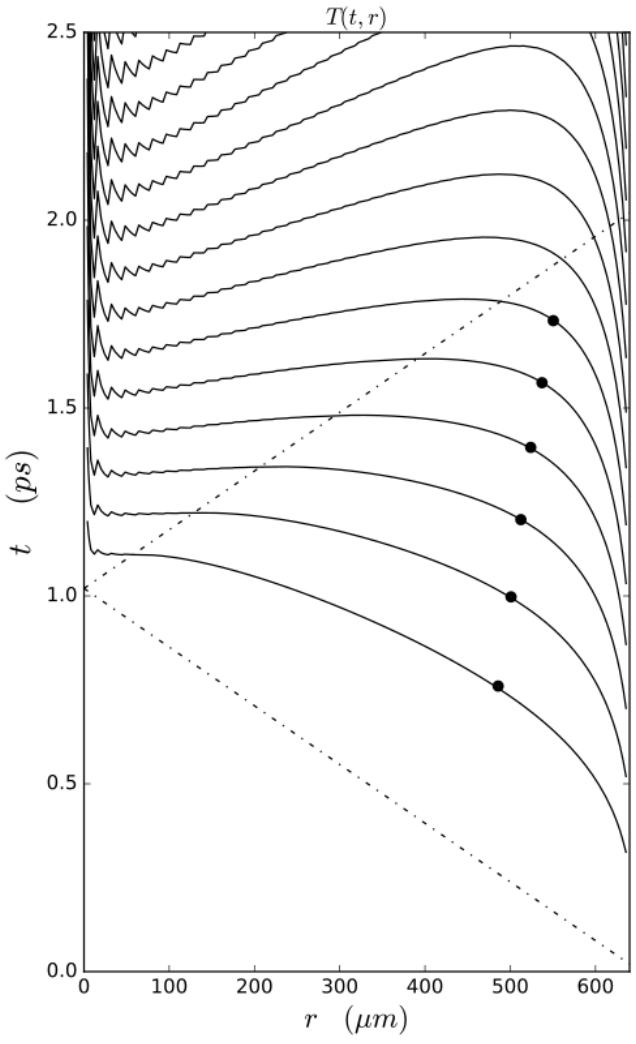

[Csernai, L.P., Kroo, N. and Papp, I. (2017). Procedure to improve the stability and efficiency of laser-fusion by nano-plasmonics method. Patent P1700278/3 of the Hungarian Intellectual Property Office.]

$\alpha_{k_{middle}} \approx 4 \times \alpha_{k_{edge}}$

Simultaneous volume ignition is up to 73%

Flat target, two sided shot

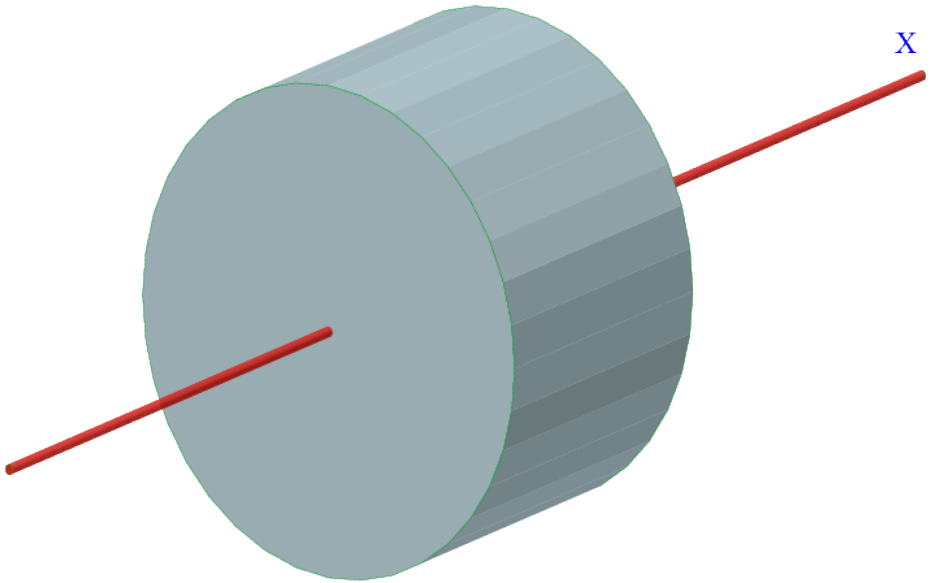

Schematic view of the cylindrical, flat target of radius, R, and thickness, h.

$V = 2\pi R^3, \qquad R = \sqrt[3]{V/(2\pi)}, \qquad h = \sqrt[3]{4V/\pi}.$

[L.P. Csernai, M. Csete, I.N. Mishustin, A. Motornenko, I. Papp, L.M. Satarov, H. Stöcker & N. Kroó, Radiation- Dominated Implosion with Flat Target, *Physics and Wave Phenomena*, **28** (3) 187-199 (2020)]

Flat target, two sided shot

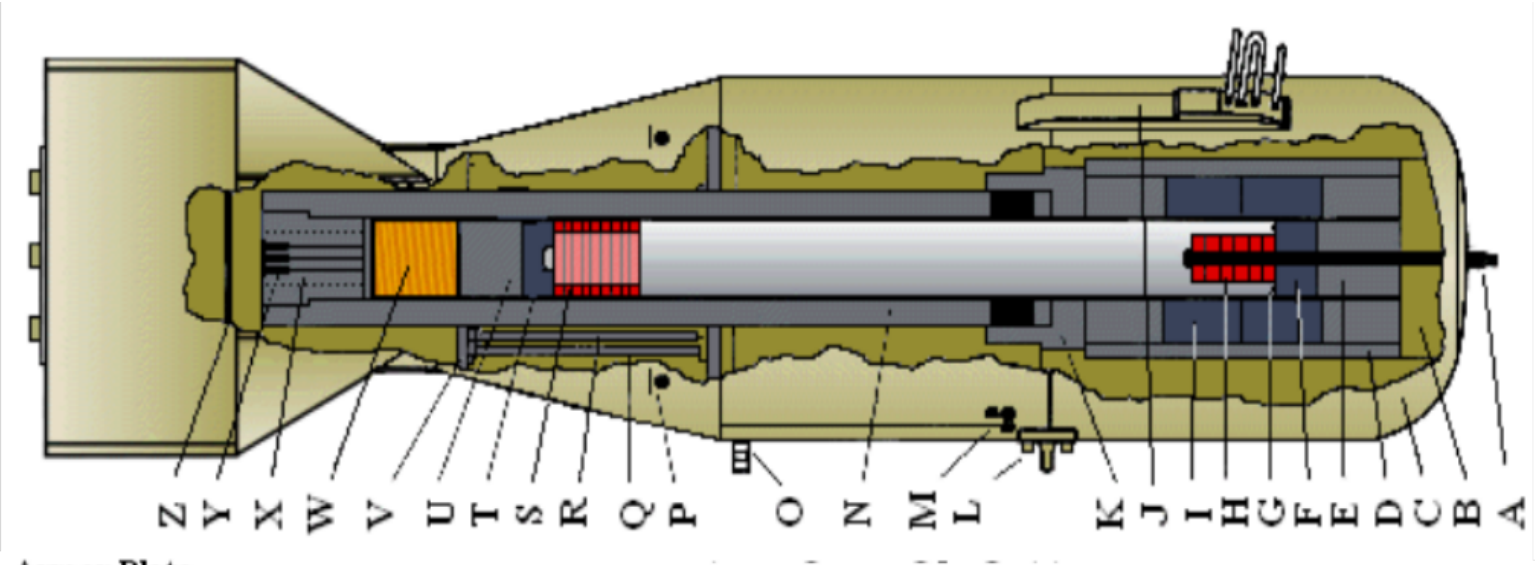

Z) Armor Plate
Y) Mark XV electric gun primers (3)
X) Gun breech with removable inner plug
W) Cordite powder bags (4)
V) Gun tube reinforcing sleeve
U) Projectile steel back
T) Projectile Tungsten-Carbide disk
S) U-235 projectile rings (9)
R) Alignment rod (3)
Q) Armored tube containing primer wiring (3)
P) Baro ports (8)
O) Electrical plugs (3)
N) 6.5" bore gun tube
M) Safing/arming plugs (3)
L) Lift lug
K) Target case gun tube adapter
J) Yagi antenna assembly (4)
I) Four-section 13" diameter Tungsten-Carbide tamper cylinder sleeve
H) U-235 target rings (6)
G) Polonium-Beryllium initiators (4)
F) Tungsten-Carbide tamper plug
E) Impact absorbing anvil
D) K-46 steel target liner sleeve
C) Target case forging
B) 15" diameter steel nose plug forging
A) Front nose locknut attached to 1" diameter main steel rod holding target components

Laser wakefield collider

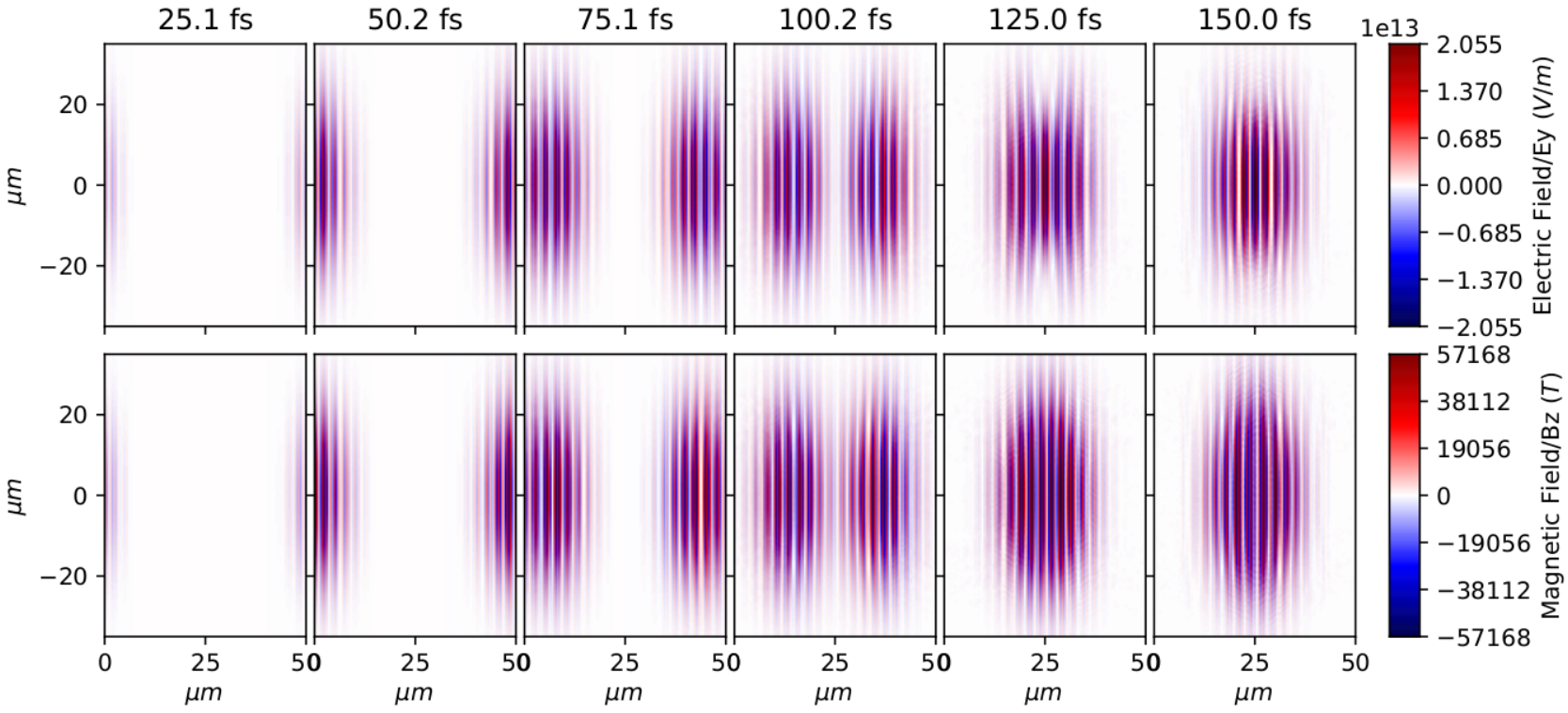

Laser parameters:

wavelength of $\lambda = 1\mu$m, full pulse length $\Delta_t = 52$fs, focus diameter is $2R = 40\mu$m, $3.0 \cdot 10^{19}$ W/cm^2 top intensity.

Laser wakefield collider

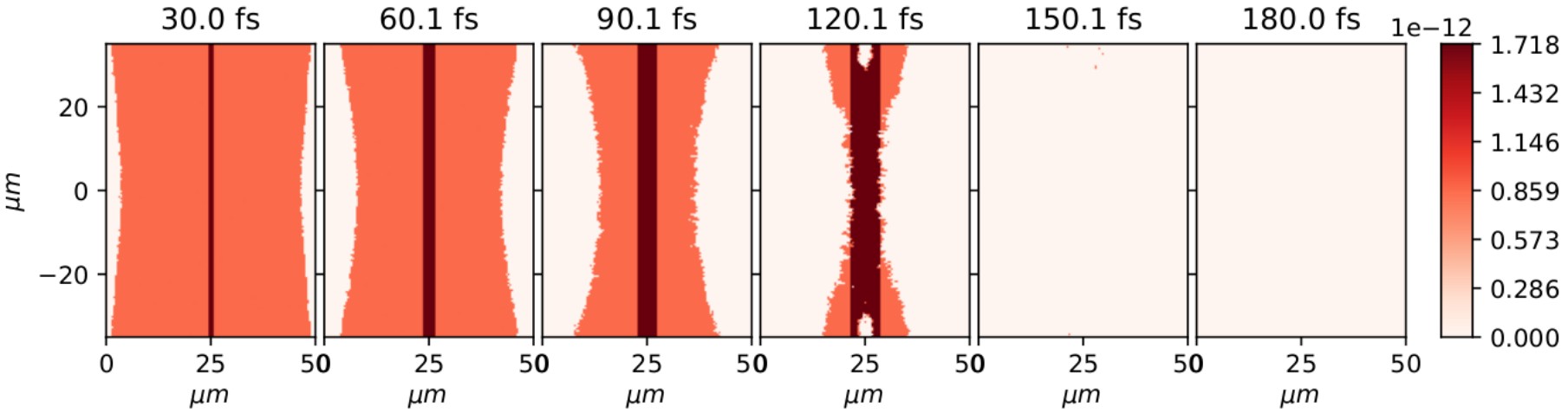

The ionization of the H atoms in a Laser Wake Field (LWF) wave due to the irradiation from both the $\pm$ x-directions, on an initial target density of $n_H = 2.13 \cdot 10^{27}$ atoms / m^3 $= 2.13 \cdot 10^{21}$ atoms / cm^3. The energy of the H atoms in Joule [J] per marker particle is shown. The H atoms disappear as protons and electrons are created. Due to the initial momentum of the colliding H slabs, the target and projectile slabs interpenetrate each other and this leads to double energy density. Several time-steps are shown at 30 fs time difference.

Varying absorptivity, similar configuration

(a)

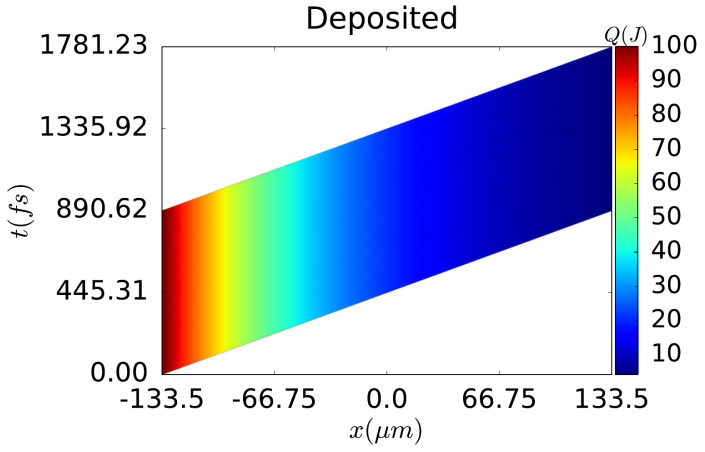

(b)

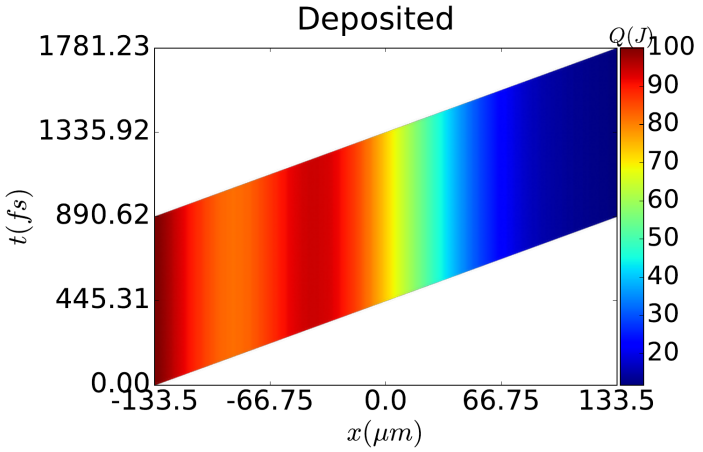

Deposited energy per unit time in the space-time plane across the depth, *h*, of the flat target. **(a) without** nano-shells **(b) with** nano-shells

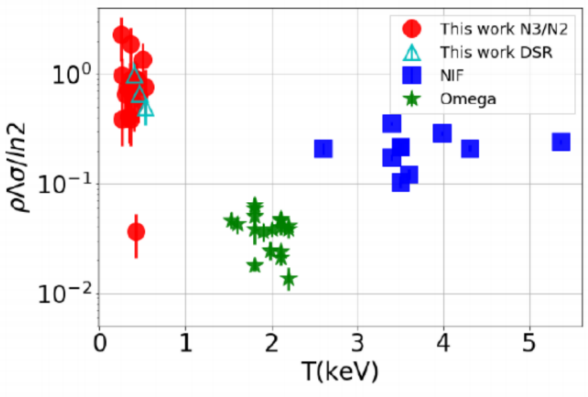

Nuclear probes of an out-of-equilibrium plasma at the highest compression

Phys. Lett. A 383 (2019) 2285-2289.

G. Zhang [a,b,*], M. Huang [c], A. Bonasera [d,e,*], Y.G. Ma [f,b,i,*], B.F. Shen [g,h,*], H.W. Wang [a,b], W.P. Wang [g], J.C. Xu [g], G.T. Fan [a,b], H.J. Fu [b], H. Xue [b], H. Zheng [j], L.X. Liu [a,b], S. Zhang [c], W.J. Li [b], X.G. Cao [a,b], X.G. Deng [b], X.Y. Li [b], Y.C. Liu [b], Y. Yu [g], Y. Zhang [b], C.B. Fu [k], X.P. Zhang [k]

Similar **two sided** shooting configuration was already scessful

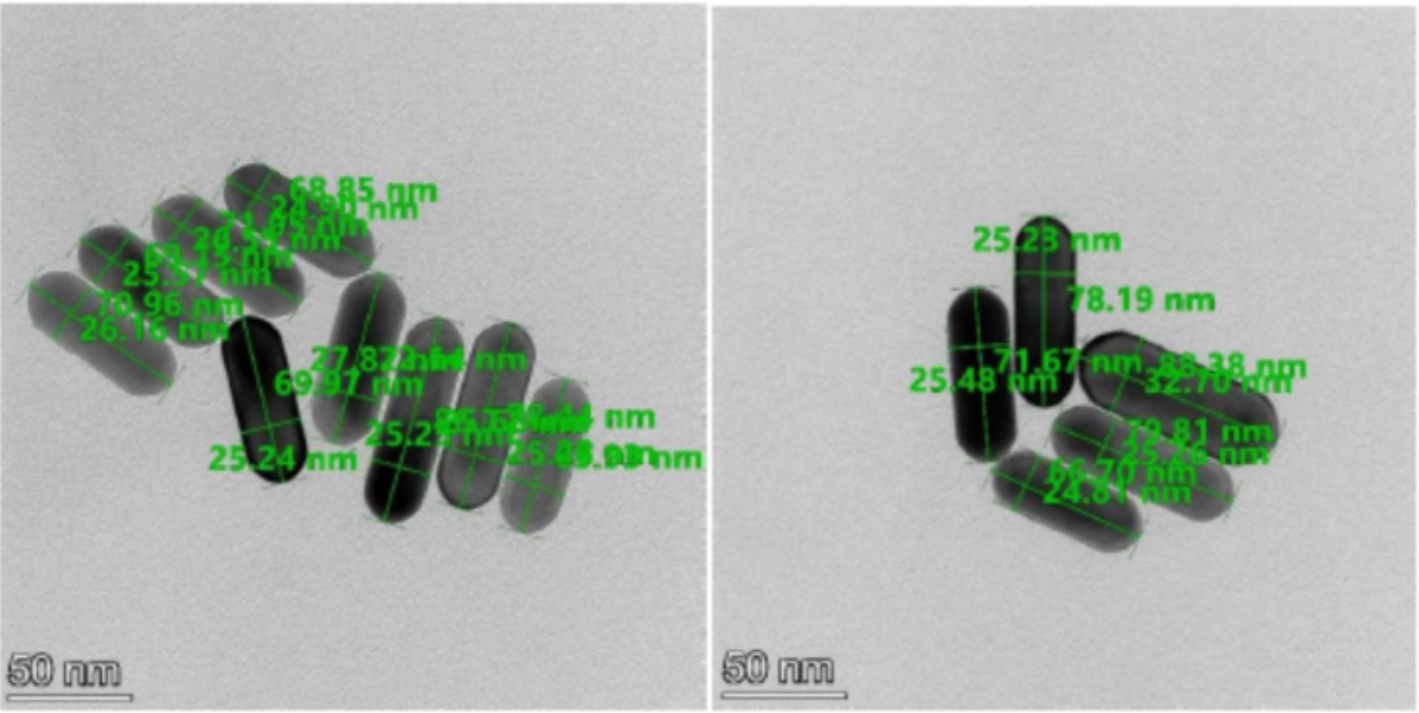

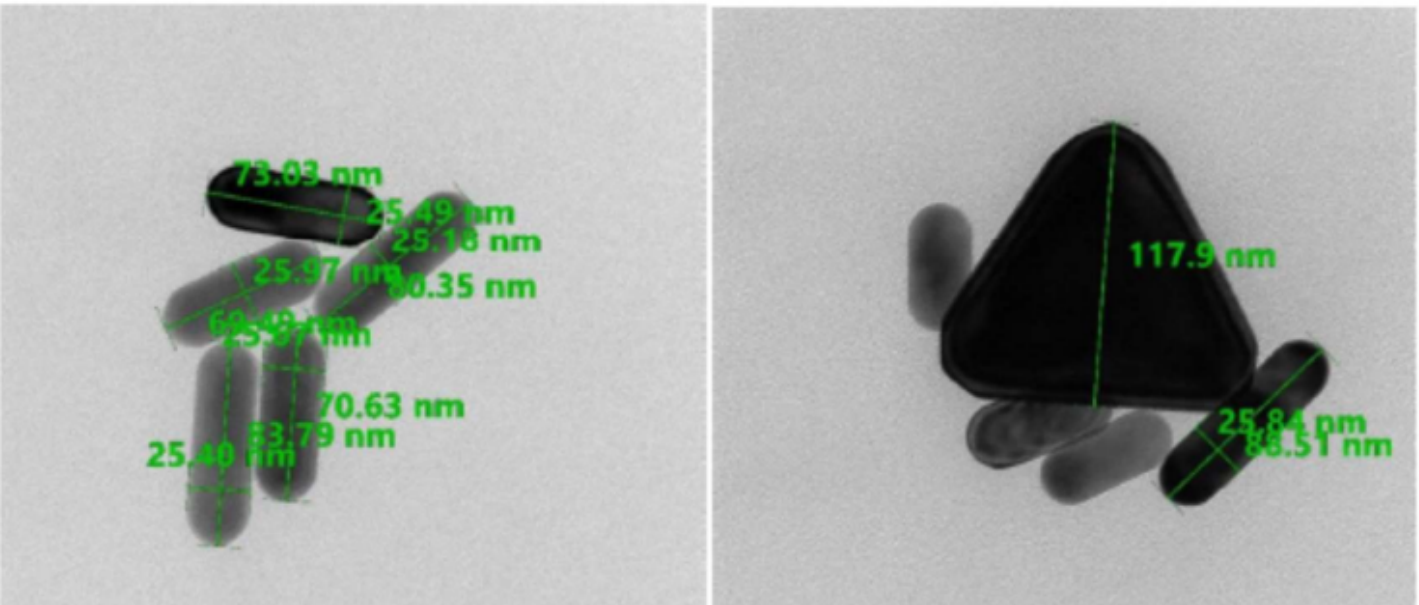

Transmission Electron-microscopy photos of 75x25 nm gold nano-rod antennas

[Judit Kámán, A. Bonyár et al. (NAPLIFE Collab.)., Gold nanorods …, 10th ICNFP 2021, **Kolymbari]**

Modelling the Nanorod

Nanorod

Field solver:

$\epsilon(\omega) = 1 - \frac{\omega_p^2}{(\omega^2 + i\gamma\omega)}$

where ω_p is the plasma frequency: $\sqrt{\frac{n_e e^2}{m' \epsilon_0}}$

γ is the damping factor or collision frequency: $\gamma = \frac{1}{\tau}$ and τ is the average time between collisions

Particle simulation:

$$\frac{\partial \boldsymbol{E}}{\partial t} = \frac{1}{\mu_0 \epsilon_0} \nabla \times \boldsymbol{B} - \frac{\boldsymbol{J}}{\epsilon_0}, \quad \frac{\partial \boldsymbol{B}}{\partial t} = -\nabla \times \boldsymbol{E}$$

$\gamma_i m_i \boldsymbol{v}_i = q_i(\boldsymbol{E}_i + \boldsymbol{v}_i \times \boldsymbol{B}_i)$, γ_i is the relativistic factor

Nanorod

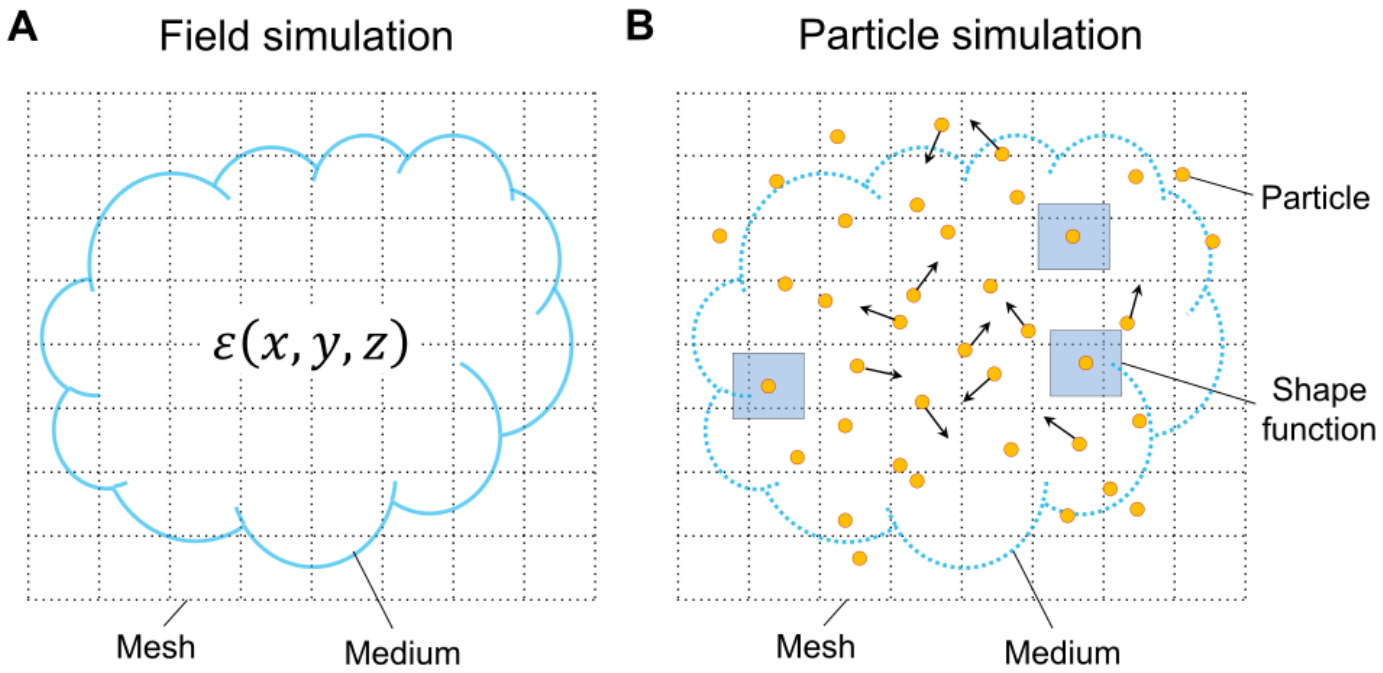

[W. J. Ding,et al., Particle simulation of plasmons Nanophotonics, vol. 9, no. 10, pp. 3303-3313 (2020)]

Particle In Cell methods

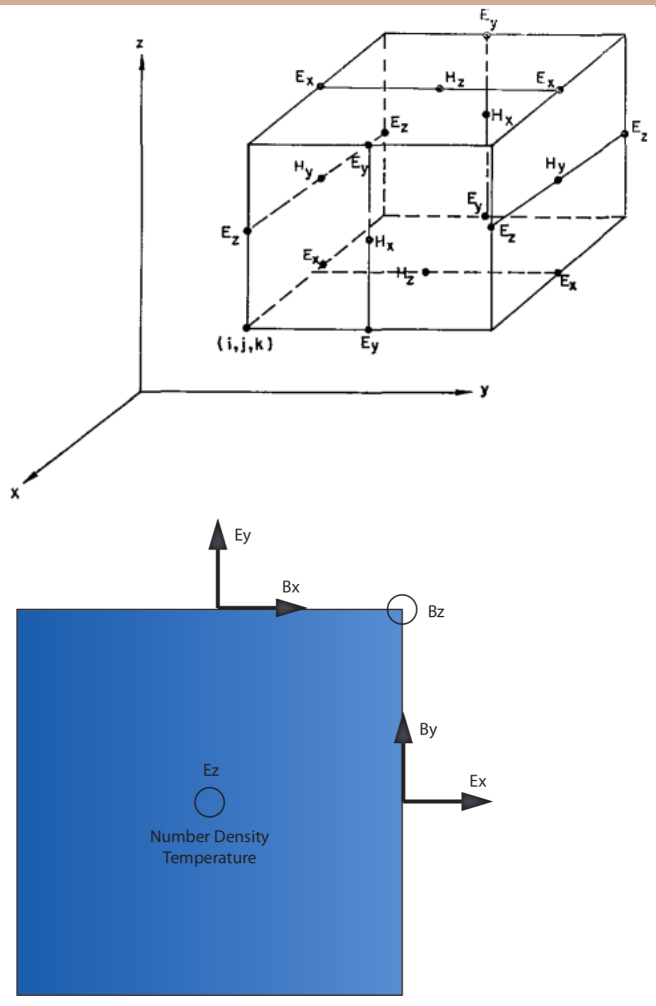

Figure 2: The Yee grid in 2D

[F.H. Harlow (1955). A Machine Calculation Method for Hydrodynamic Problems. Los Alamos Scientific Laboratory report LAMS-1956]

[T.D. Arber et al 2015 Plasma Phys. Control. Fusion 57 113001]

A **super-particle** (**marker-particle**) is a computational particle that represents many real particles.

Particle **mover** or **pusher** algorithm as (typically Boris algorithm).

Finite-difference time-domain method for solving the time evolution of **Maxwell's equations**.

Particle shape

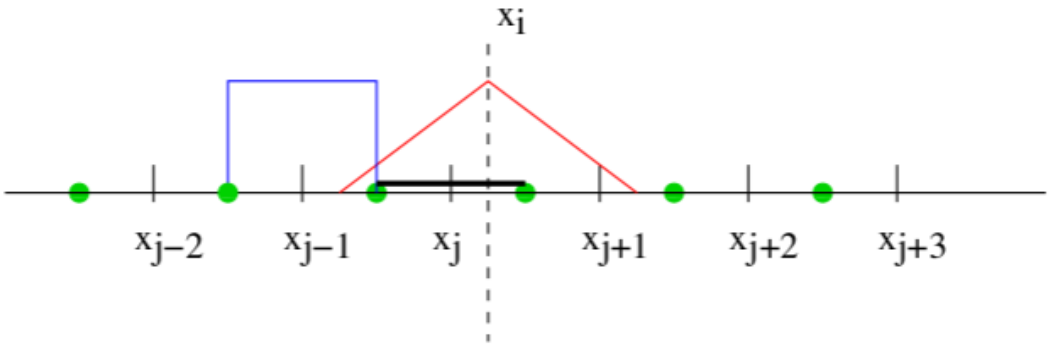

Figure 3: Second order particle shape function

First order approximations are considered

$$F_{part} = \frac{1}{2}F_{i-1}\left(\frac{1}{2} + \frac{x_i - X}{\Delta x}\right)^2 + \frac{1}{2}F_i\left(\frac{3}{4} - \frac{(x_i - X)^2}{\Delta x^2}\right)^2 + \frac{1}{2}F_{i+1}\left(\frac{1}{2} + \frac{x_i - X}{\Delta x}\right)^2$$

[EPOCH 4.0 dev manual]

FDTD in EPOCH

- $\boldsymbol{E}_{n+\frac{1}{2}} = \boldsymbol{E}_n + \frac{\Delta t}{2}\left(c^2\nabla \times \boldsymbol{B}_n - \frac{\boldsymbol{j}_n}{\epsilon_0}\right)$
- $\boldsymbol{B}_{n+\frac{1}{2}} = \boldsymbol{B}_n - \frac{\Delta t}{2}\left(\nabla \times \boldsymbol{E}_{n+\frac{1}{2}}\right)$
- Call particle pusher which calculates j_{n+1}
- $\boldsymbol{B}_{n+1} = \boldsymbol{B}_{n+\frac{1}{2}} - \frac{\Delta t}{2}\left(\nabla \times \boldsymbol{E}_{n+\frac{1}{2}}\right)$
- $\boldsymbol{E}_{n+1} = \boldsymbol{E}_{n+\frac{1}{2}} + \frac{\Delta t}{2}\left(c^2\nabla \times \boldsymbol{B}_{n+1} - \frac{\boldsymbol{j}_{n+1}}{\epsilon_0}\right)$

Particle pusher

- Solves the relativistic equation of motion under the Lorentz force for each marker-particle

$$\boldsymbol{p}_{n+1} = \boldsymbol{p}_n + q\Delta t \left[\boldsymbol{E}_{n+\frac{1}{2}} \left(\boldsymbol{x}_{n+\frac{1}{2}} \right) + \boldsymbol{v}_{n+\frac{1}{2}} \times \boldsymbol{B}_{n+\frac{1}{2}} \left(\boldsymbol{x}_{n+\frac{1}{2}} \right) \right]$$

  $\boldsymbol{p}$ is the particle momentum q is the particle's charge $\boldsymbol{v}$ is the velocity.
  $\boldsymbol{p} = \gamma m \boldsymbol{v}$, where m is the rest mass $\gamma = \left[(\boldsymbol{p}/mc)^2 + 1 \right]^{1/2}$

- Villasenor and Buneman current deposition scheme [Villasenor J & Buneman O 1992 Comput. Phys. Commun. 69 306], always satisfied: $\nabla \cdot \boldsymbol{E} = \rho/\epsilon_0$, where ρ is the charge density.

Metal Nanoparticles as Plasmas

The conduction band electrons in metals behave as strongly coupled plasmas.

For golden nanorods of 25nm diameter in vacuum this gives an effective wavelength of $\lambda_{eff} = 266\text{nm}$

$$\frac{\lambda_{eff}}{2R\pi} = 13.74 - 0.12[\varepsilon_\infty + 141.04] - \frac{2}{\pi} + \frac{\lambda}{\lambda_p} 0.12\sqrt{\varepsilon_\infty + 141.04}$$

[Lukas Novotny, Effective Wavelength Scaling for Optical Antennas, Phys. Rev. Lett. **98**, 266802 (2007).]

Considerations for the simulation box

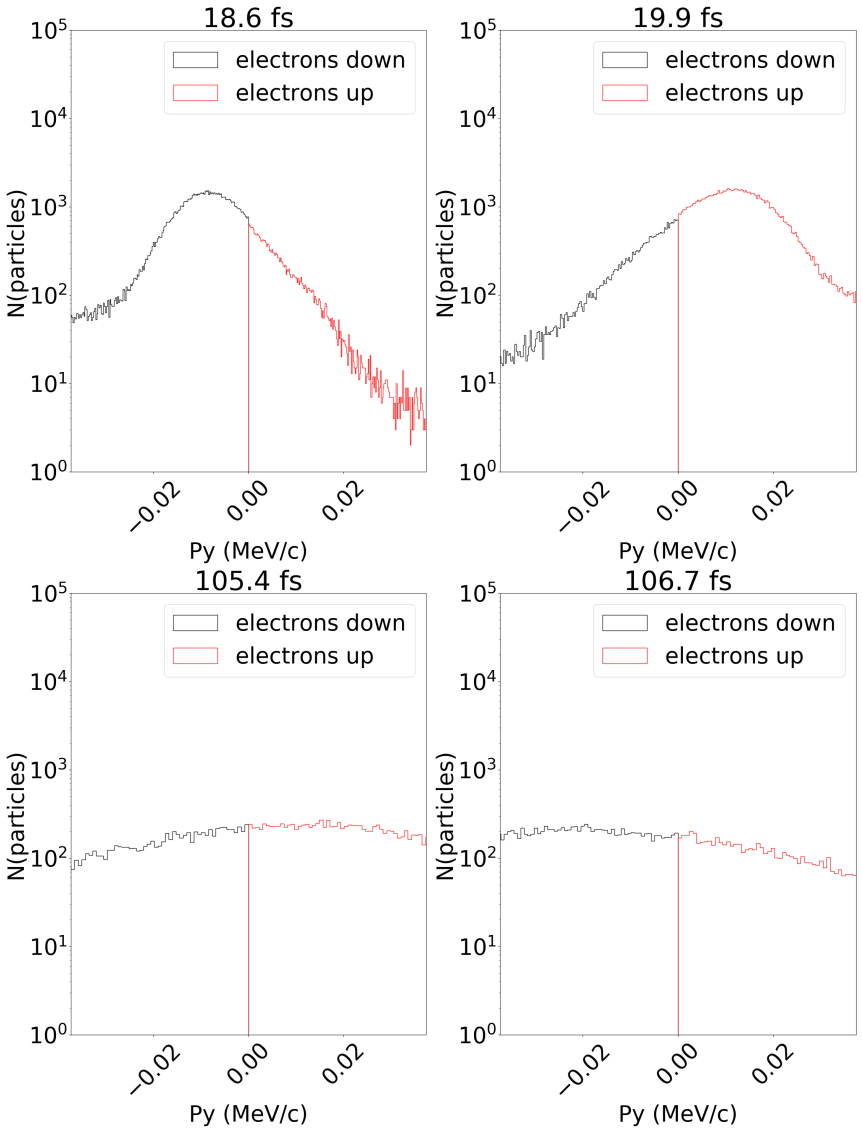

Considerations for the simulation box:
$S_{CB} = 530 \times 530\text{nm}^2 = 2.81 \times 10^{-9}\text{cm}^2$ and length of $L_{CB} = 795\text{nm}$

beam crosses the box in $T = 795\text{nm}/c = 2.65\text{fs}$

Nanorod size: 25 nm diameter with 130 nm length

Pulse length: $40 \times \lambda/c = 106$ fs
Intensity: 4×10^{15} W/cm^2
[Papp I, Bravina L, Csete M, Kumari A, et al. Kinetic model evaluation of the resilience of plasmonic nanoantennas for laser-induced fusion. PRX Energy (2022)]

Ideal world: orthogonal to beam line

Nanorod inside a PIC simulation box

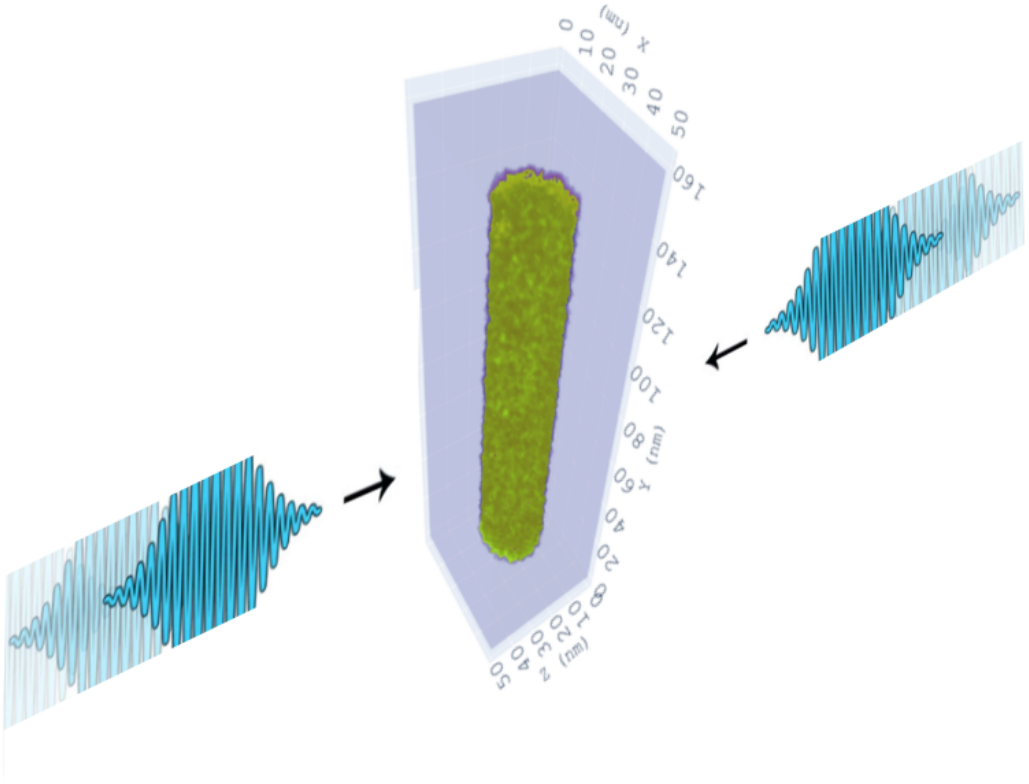

Evolution of the nanoantenna

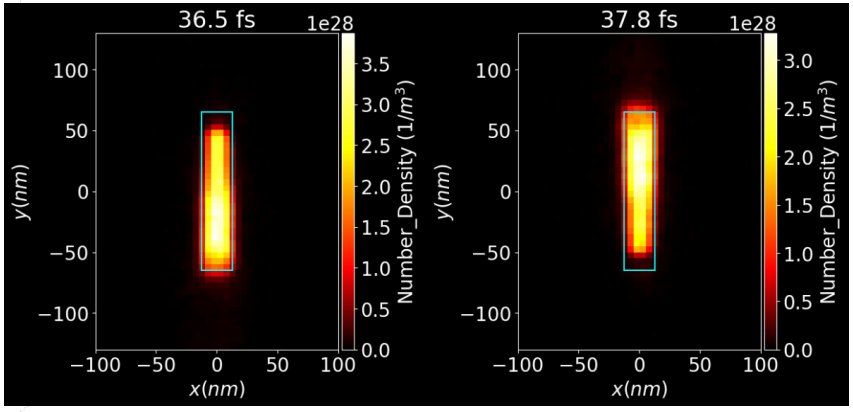

Number density of electrons in the middle of a nanorod of size 25x130 nm at different times. The nanorod is orthogonal to the beam direction, x.

Kinetic Modelling of the Nanorod in Vacuum

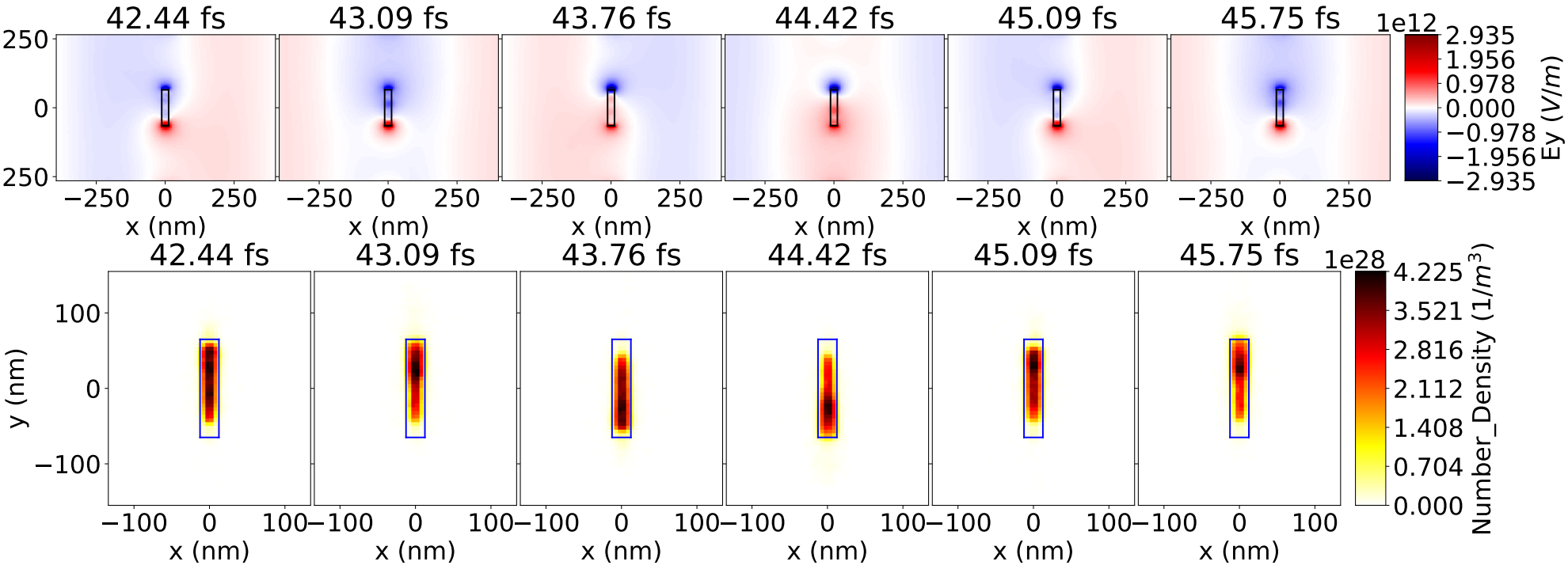

- Evolution of the E field's y component from 42.4 till 45.7 fs, around a nanorod of 25x130 nm.

- The direction of the E field at the two ends of the nanorod does not change.

Metal Nanoparticles as Plasmas in UDMA-Tegdma

For golden nanorods of 25nm diameter in vacuum this gives an effective wavelength of $\lambda_{eff}/2 = 85\text{nm}$

The **propagation** velocity of light **inside** the **medium** is reduced to $c_s = c/\sqrt{\varepsilon_s}$, where $\varepsilon_s = n^2$.

$$\frac{\lambda_{eff}}{2R\pi} = 13.74 - 0.12[\varepsilon_\infty + \varepsilon_s 141.04]/\varepsilon_s$$
$$-\frac{2}{\pi} + \frac{\lambda}{\lambda_p} 0.12\sqrt{\varepsilon_\infty + \varepsilon_s 141.04}/\varepsilon_s$$

[Lukas Novotny, Effective Wavelength Scaling for Optical Antennas, Phys. Rev. Lett. **98**, 266802 (2007).]

Real world: scattered

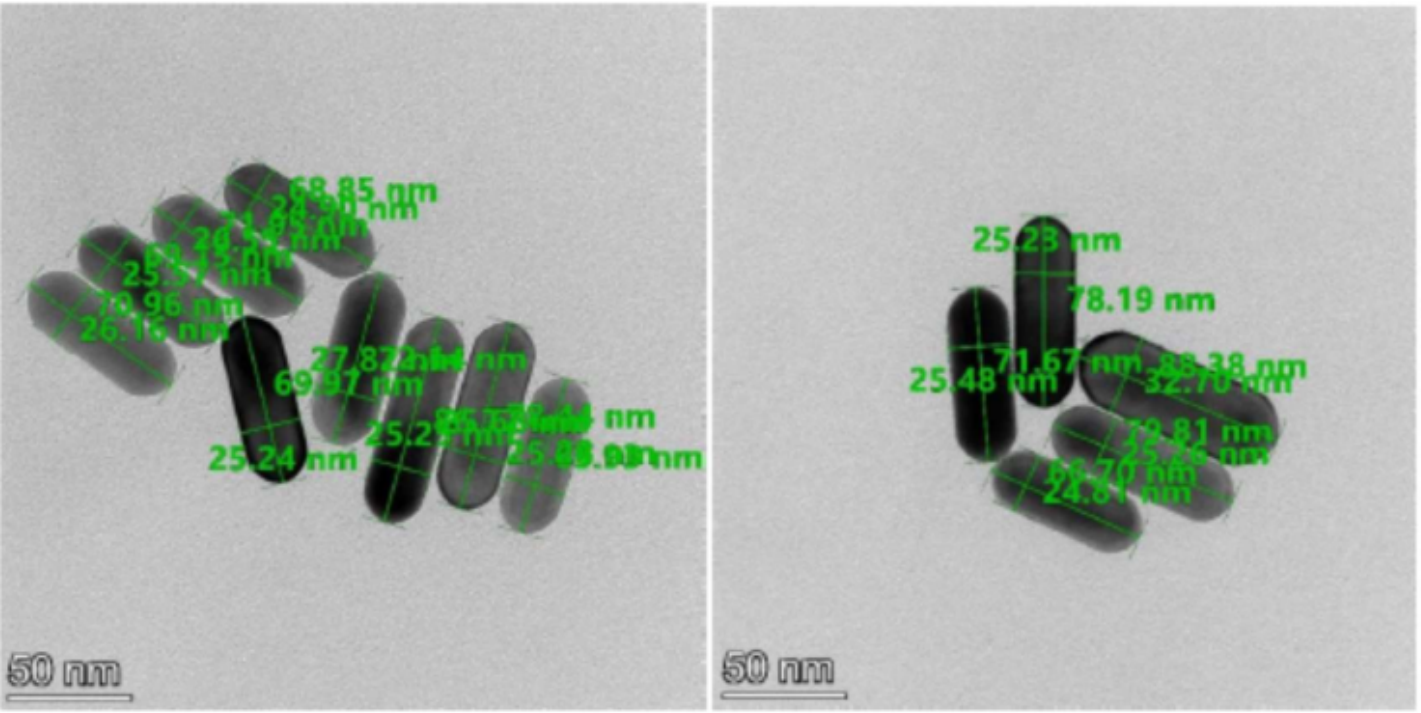

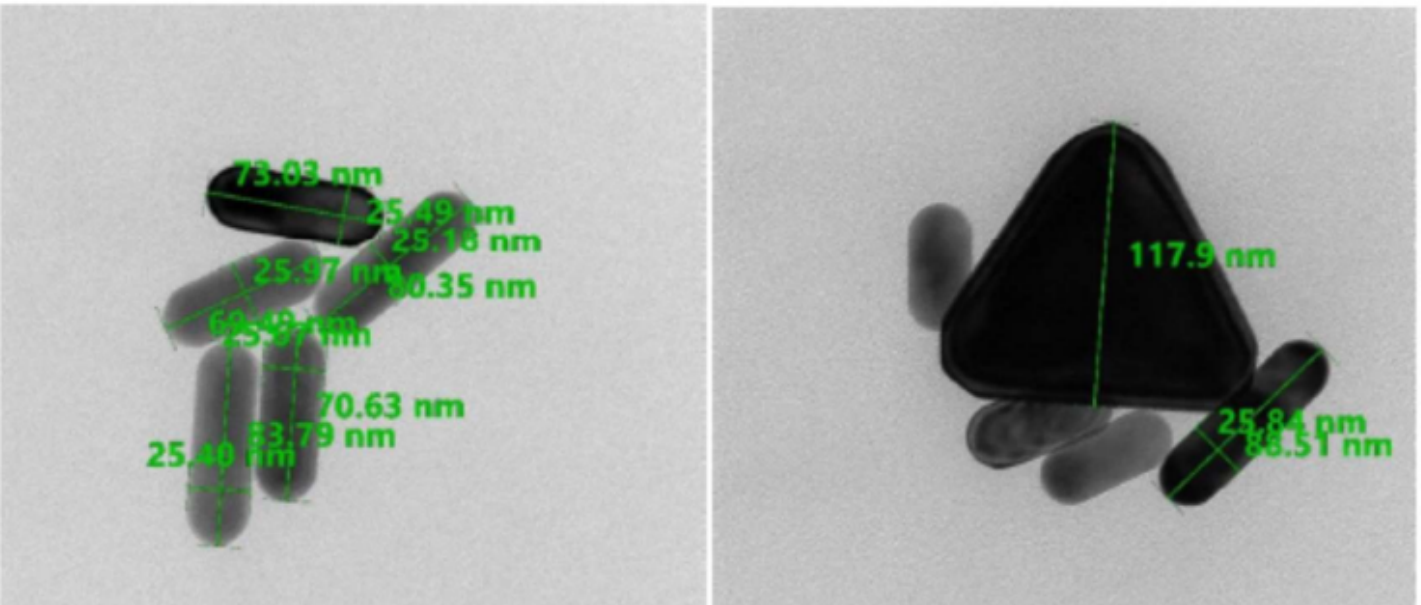

Transmission Electron-microscopy photos of 75x25 nm gold nano-rod antennas

[Judit Kámán, A. Bonyár et al. (NAPLIFE Collab.)., Gold nanorods …, 10th ICNFP 2021, **Kolymbari]**

Out of resonance (UDMA-TEGDMA copolymer)

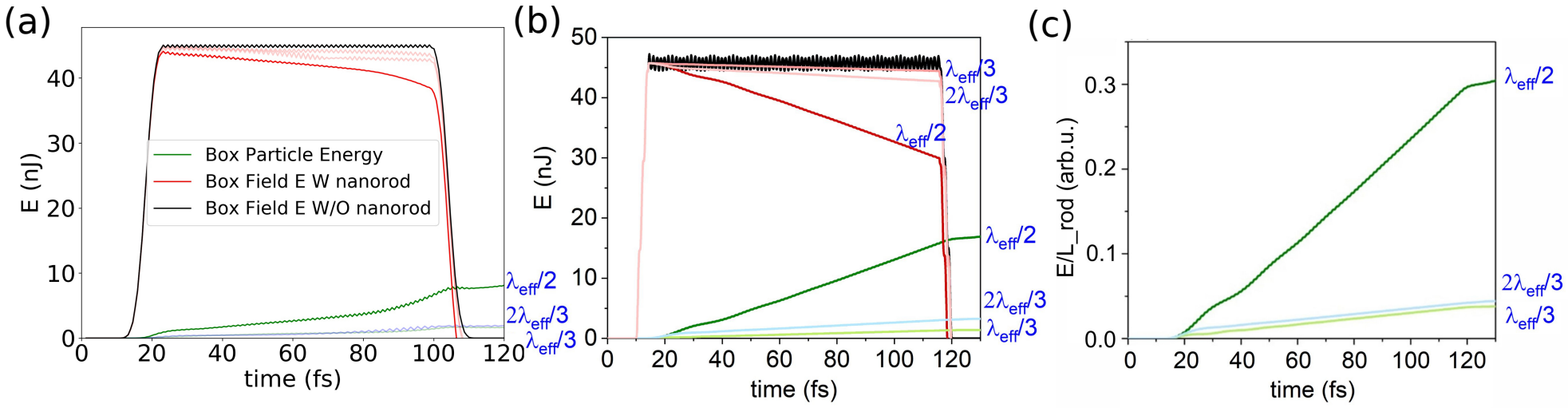

Optical response of the gold nanorod with different numerical methods and lengths, $L = \lambda_{eff}/2, \lambda_{eff}/3 and 2\lambda_{eff} eff/3$. (a) PIC, (b) FEM and (c) FEM with normalized values to unit antenna length.

[I. Papp, L. Bravina, M. Csete, et al.(NAPLIFE Collaboration), Kinetic model of resonant nanoantennas in polymer for laser induced fusion, Frontiers in Physics, **11**, 1116023 (2023).]

Comparing orientation, shapes and sizes

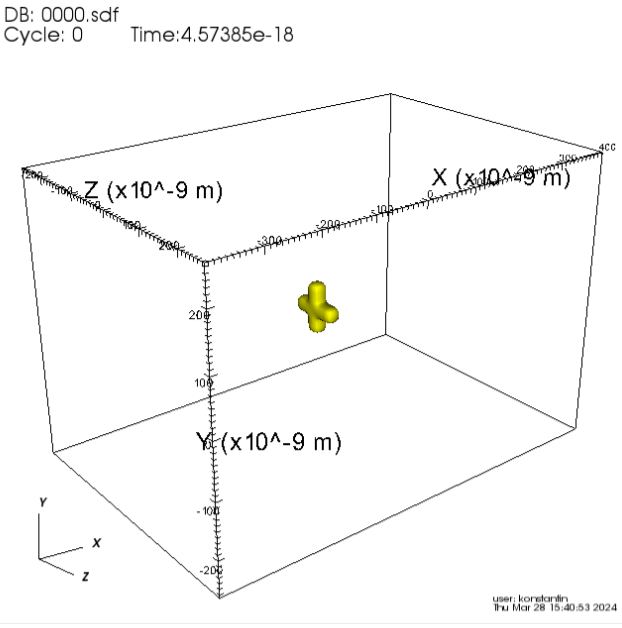

a

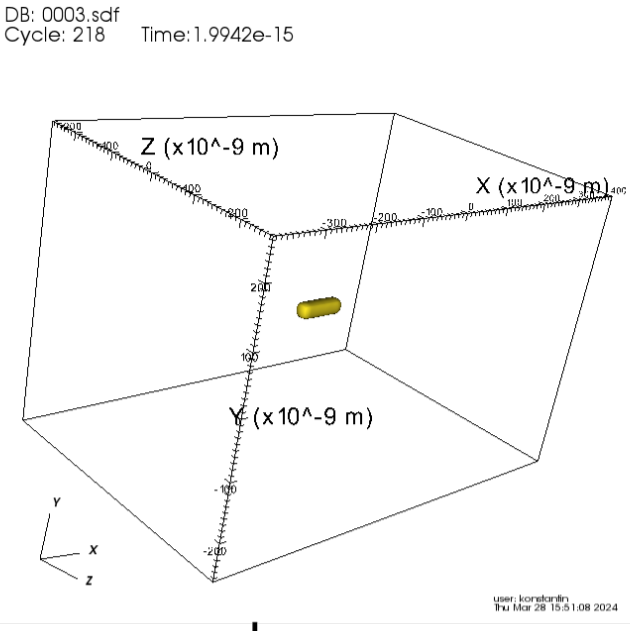

b

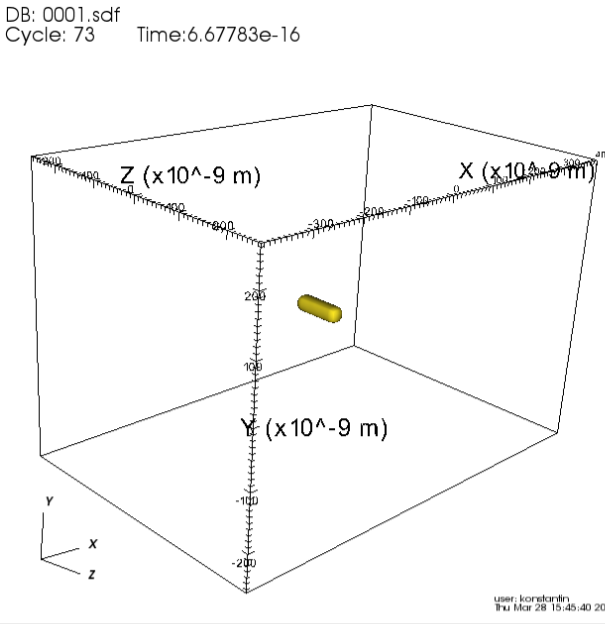

c

- We submerged the nanorods in Hydrogen medium
- Species were separately defined: conducting electrons, Au ions, H atoms, protons (H after ionized) and H electrons
- (a) **crossed** quadruple (b) **along** the beam direction (c) **laying** or sleeping policeman

[See presentation of Prof. K. Zhukovsky]

Comparing orientation, shapes and sizes

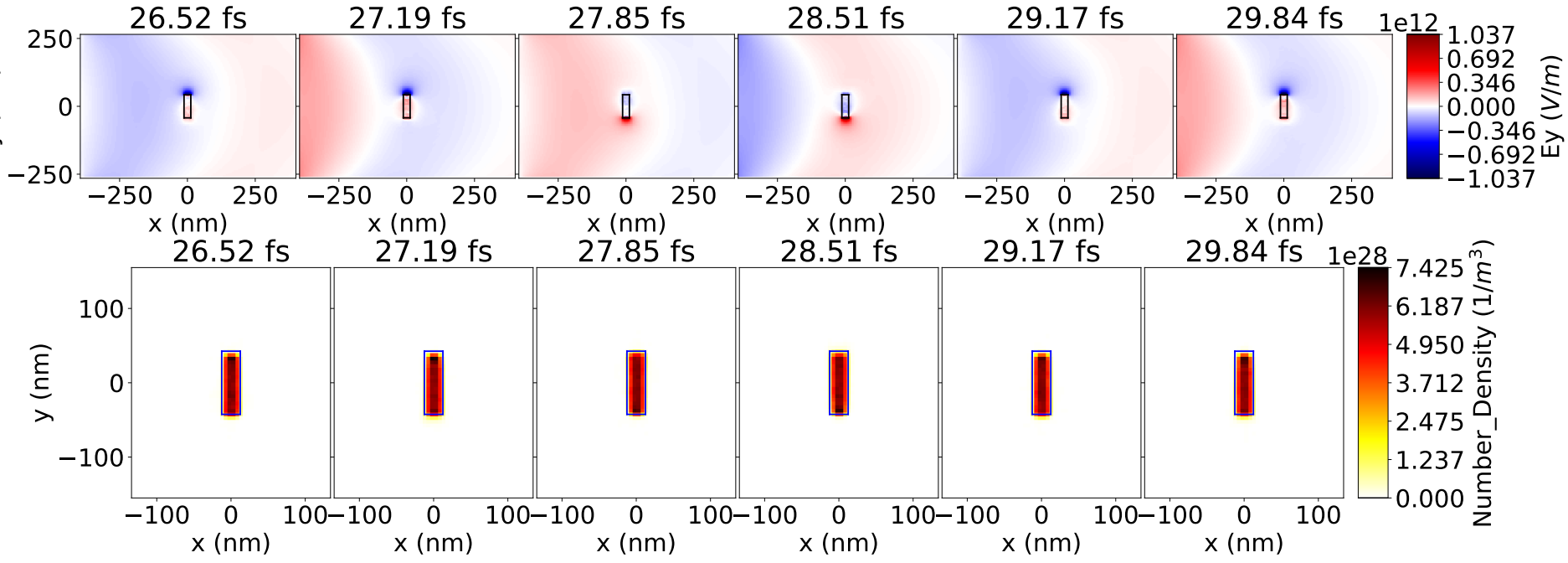

- Evolution of the E field's **polarization direction** component from 42.4 till 45.7 fs, around a nanorod of 25x85 nm. $I = 4 \cdot 10^{15} \mathrm{W/cm^2}$
- Also side view of the proper conducting electron density of dipole oriented in **parallel** with polarization direction, in quarter of a period steps.

Comparing orientation, shapes and sizes

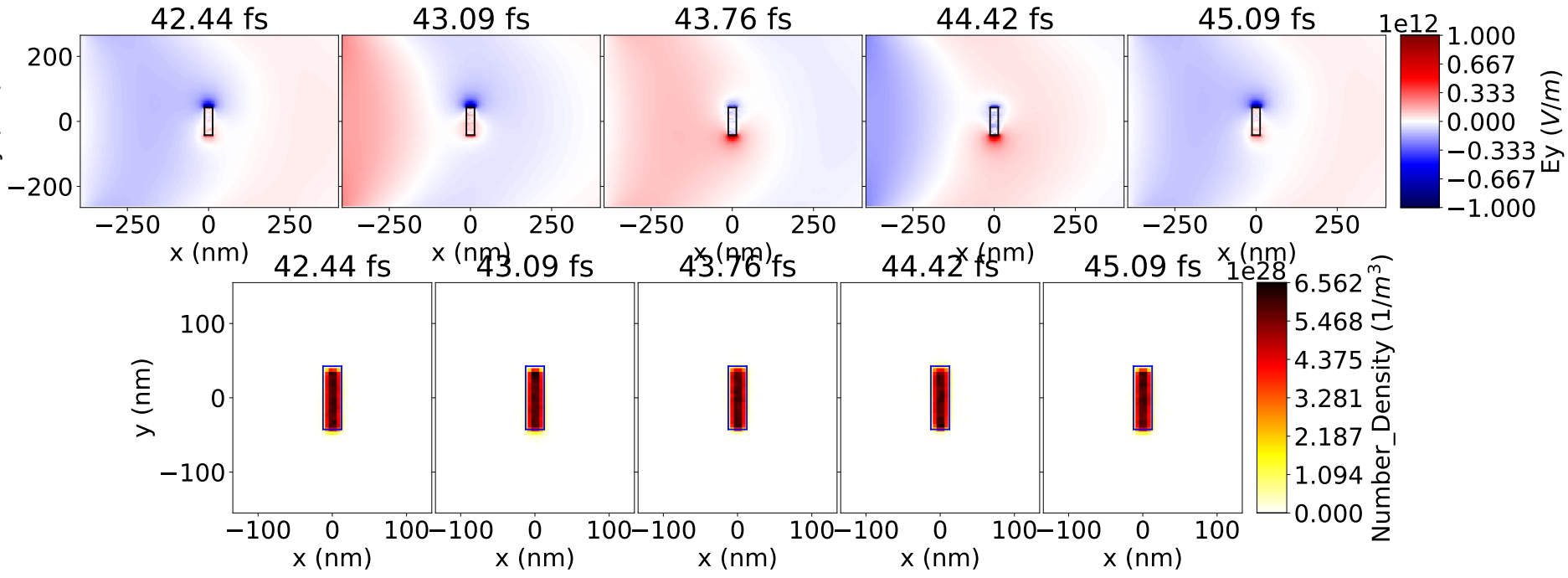

- Evolution of the E field's **polarization direction** component from 42.4 till 45.7 fs, around a **crossed quadroupole** (side view) of 25x85 nm. $I = 4 \cdot 10^{15} \mathrm{W/cm^2}$
- Also side view of the proper conducting electron density in quarter of a period steps.

Comparing orientation, shapes and sizes

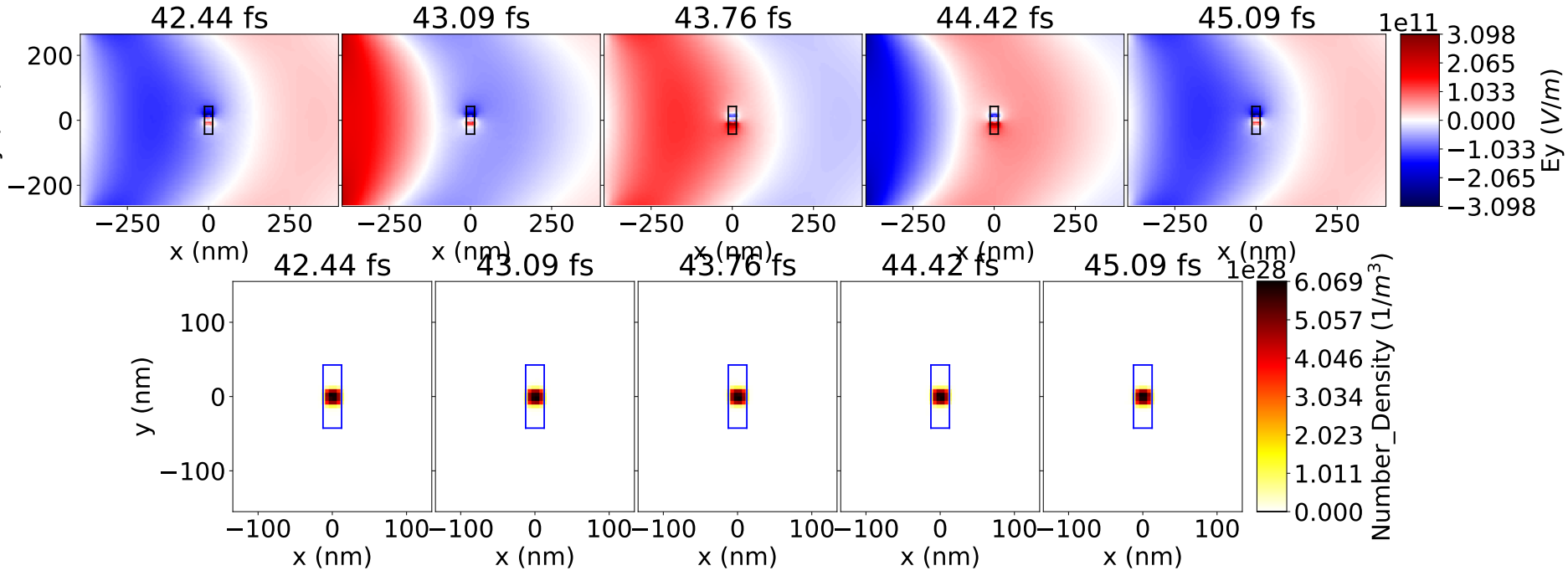

- Evolution of the E field's **polarization direction** component from 42.4 till 45.7 fs, around a "**laying**" sleeping police antenna of 25x85 nm. $I = 4 \cdot 10^{15} \mathrm{W/cm^2}$
- Also side view of the proper conducting electron density in quarter of a period steps. (Antenna is orthogonal to **both** polarization and beam direction).

Comparing orientation, shapes and sizes

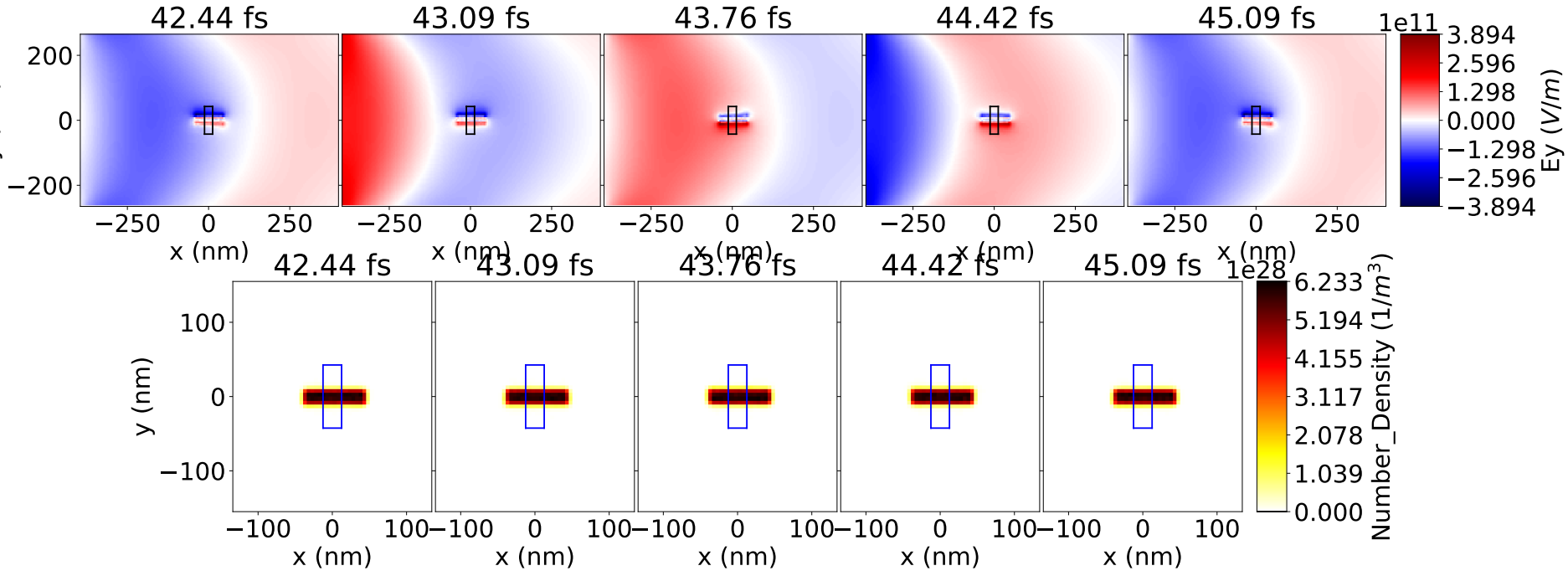

- Evolution of the E field's **polarization direction** component from 42.4 till 45.7 fs, around a nanorod of 25x85 nm. $I = 4 \cdot 10^{15} \mathrm{W/cm^2}$
- Also side view of the proper conducting electron density in quarter of a period steps. (Nanorod is parallel to the beam, orthogonal to the polarization).

Would spherical shapes be good then?

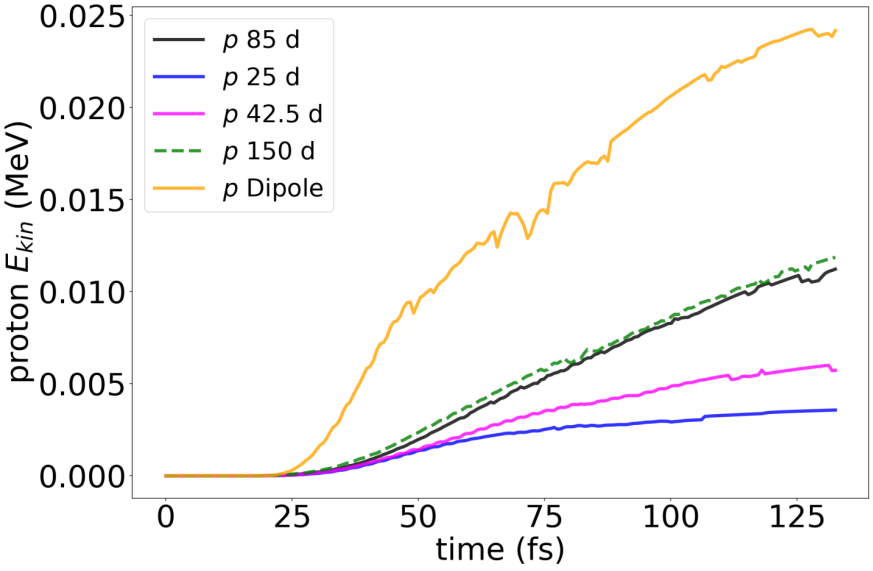

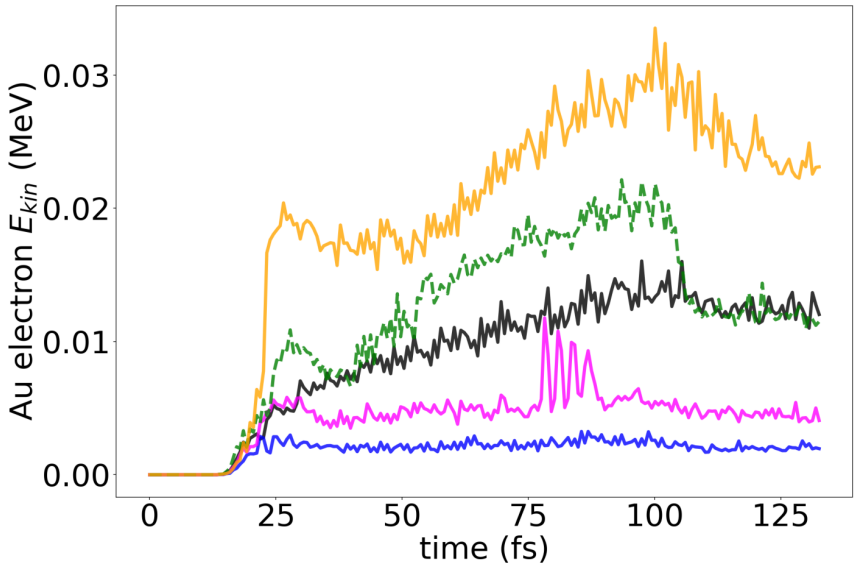

Time **evolution** of derived average **energies of** simulated ionized **Hydrogen** and **conducting electron** species of the gold nanodopes of spherical shape; diameters of dopes: 85 nm – black, 150 nm – green dashed, 42.5 nm – magenta, 25 nm – blue lines. Medium laser pulse intensities: 4×10^{15} W/cm^2 with 120 fs.

Cross checking

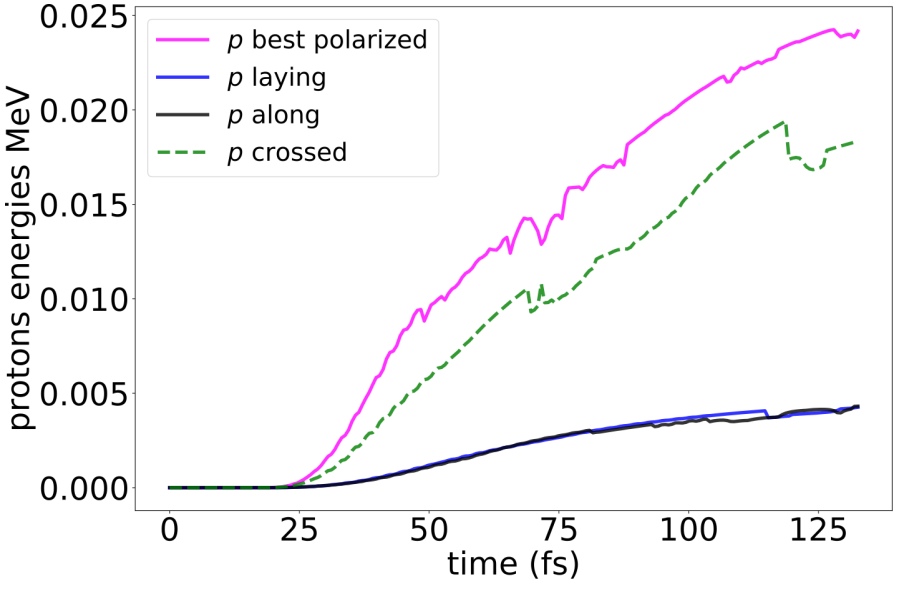

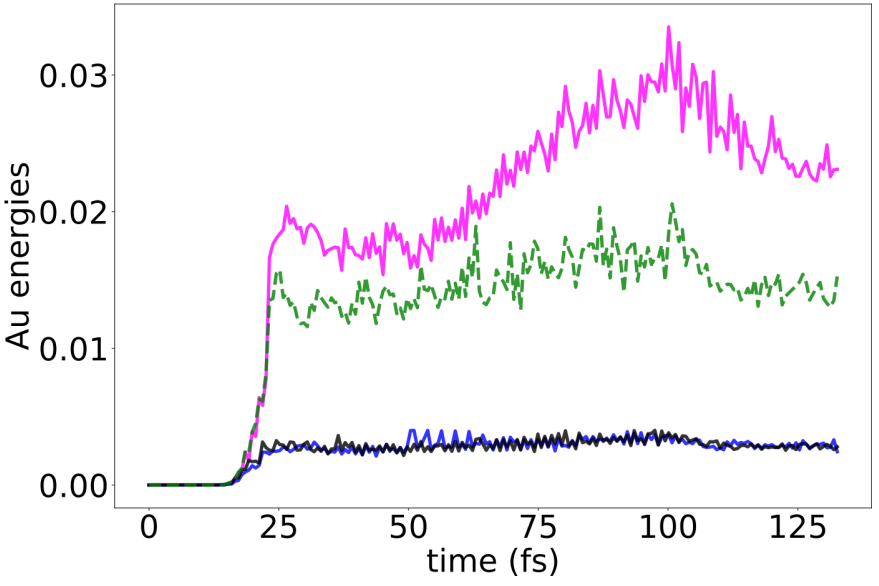

Time **evolution** of thr average **energies of** ionized **Hydrogen** and **conducting electron** species of gold nanodopes: crossed quadroupoles – green dashed, dipole of size 25x85 nm and ideal orientation along the field polarization – magenta, dipole laying across the field – blue, dipole along the pulse propagation – black lines. Medium laser pulse intensities: 4×10^{15} W/cm^2 with 120 fs.

Cross checking

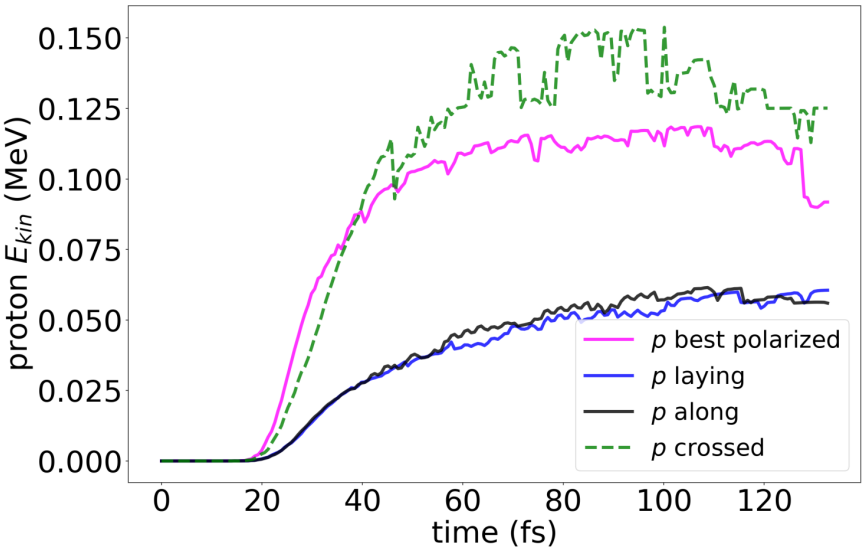

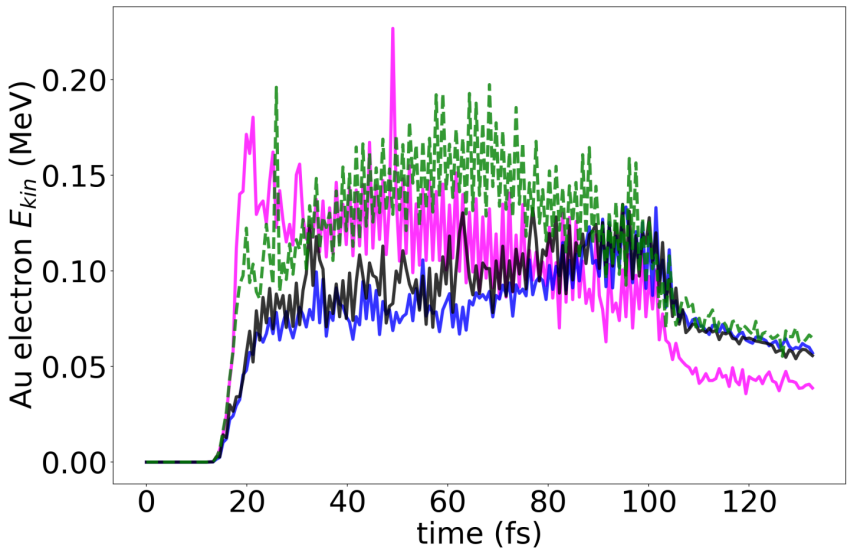

Time **evolution** of thr average **energies of** ionized **Hydrogen** and **conducting electron** species of gold nanodopes: crossed quadroupoles – green dashed, dipole of size 25x85 nm and ideal orientation along the field polarization – magenta, dipole laying across the field – blue, dipole along the pulse propagation – black lines. Medium laser pulse **intensities**: 4×10^{17} W/cm^2 with 120 fs.

Without doping

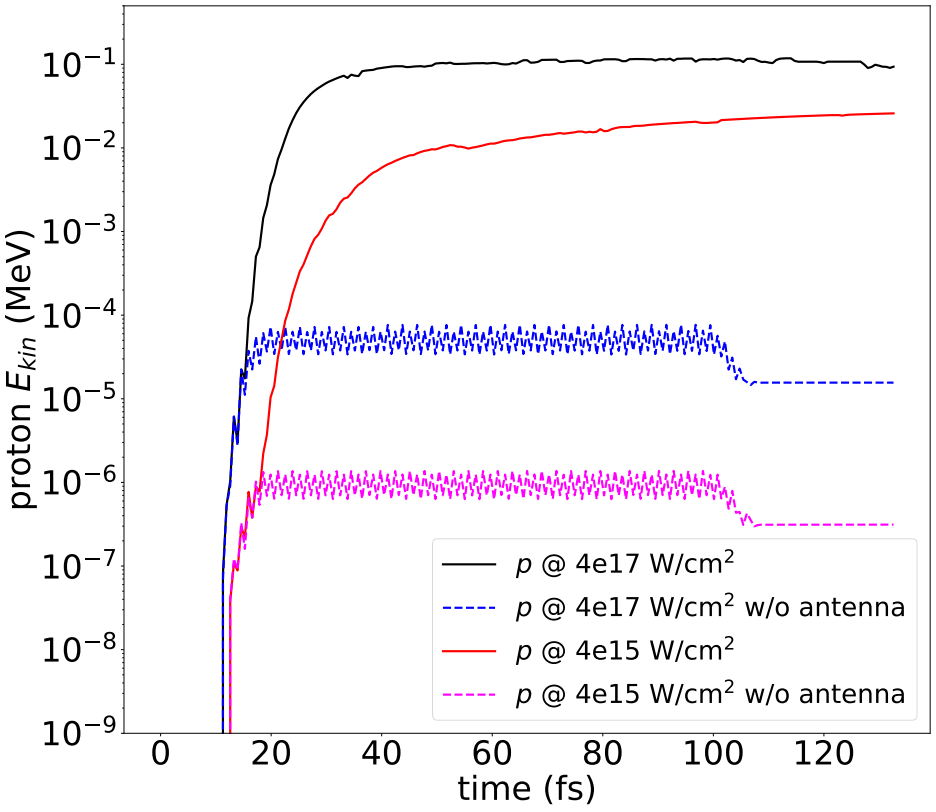

Here we show the time evolution of the derived **average kinetic** energy of the proton marker particles. In the non-doped case, for both intensities a **plateau** is reached, which lowers at the end of the shot, when no more acceleration can be achieved. However, when **nanorod** is present, the plasmonic electron bunch's motion further **accelerates** the protons by to three orders of magnitude.

One sided shooting

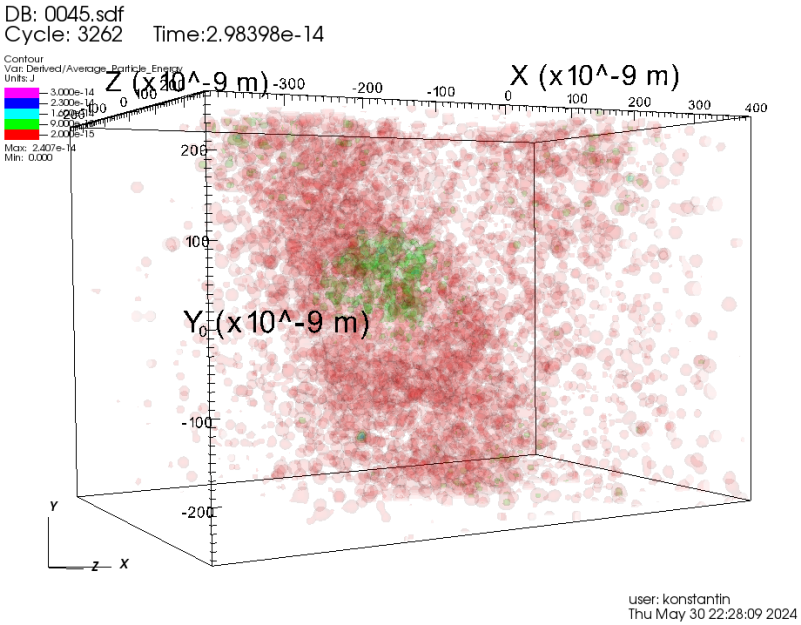

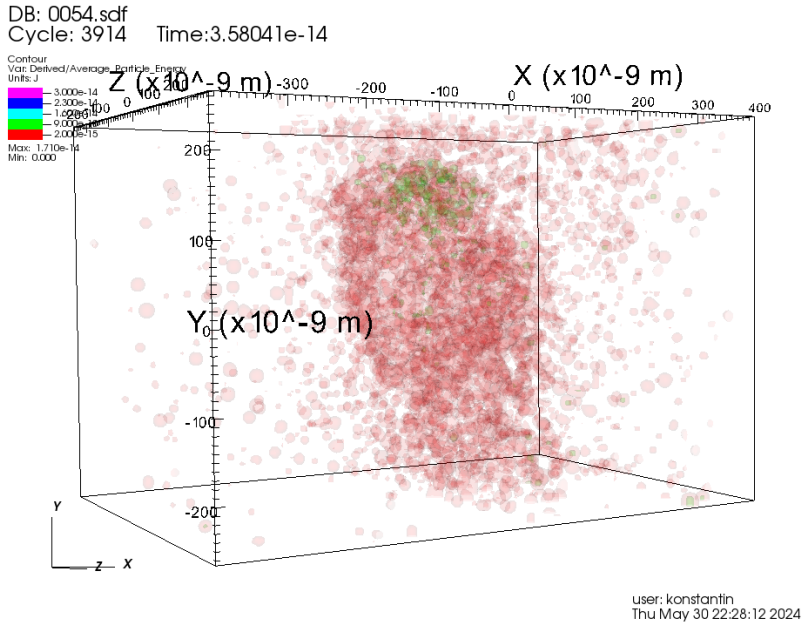

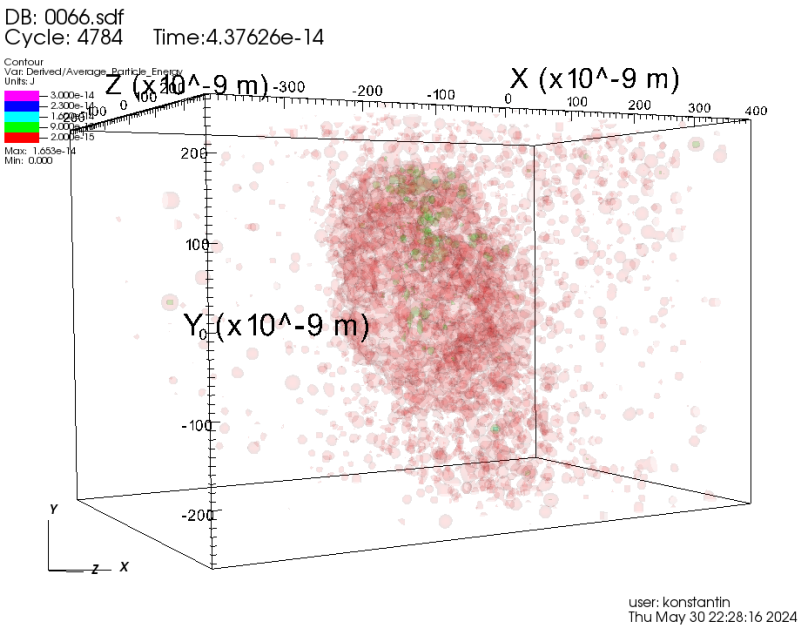

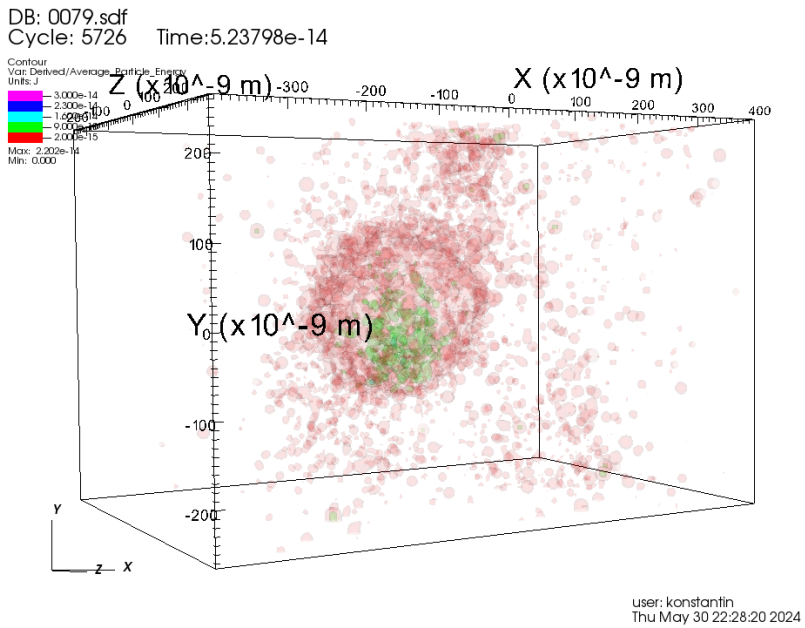

Two sided shooting

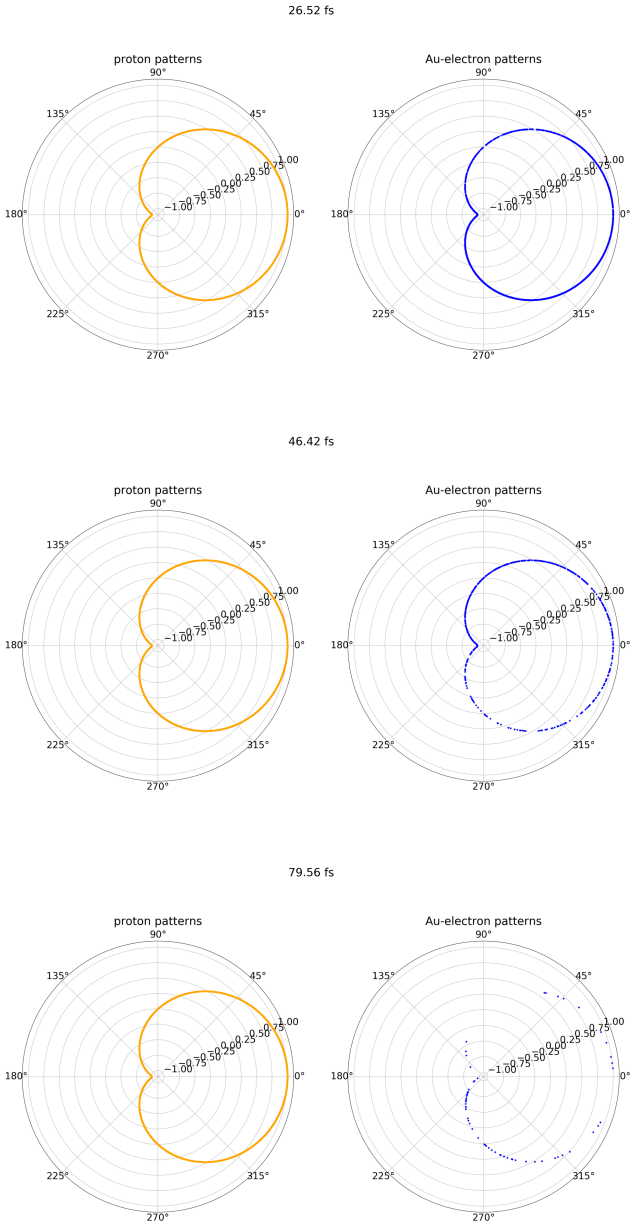

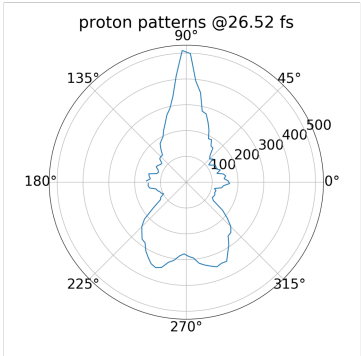

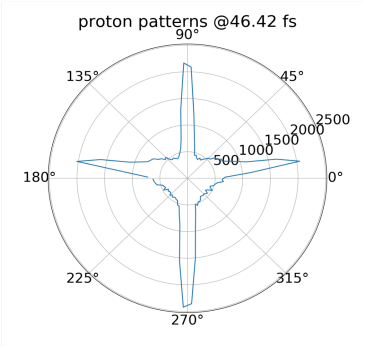

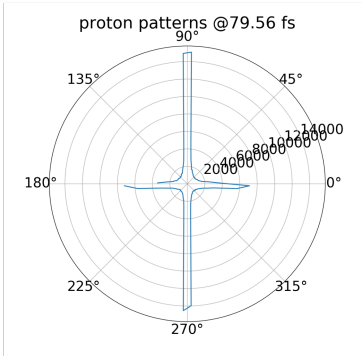

Two sided shooting

Conclusions and the future

Conclusions, Looking forward

- The model was proved to be in good agreement with currently available widely accepted methods, allowing us to confidently experiment further
- We compared various nanoantenna shapes, orientation and sizes
- Increasing radius of spherical nanoparticles increases the absorption but there is an apparent limit
- Crossed quadruples come close to the resonant dipoles, moreover at higher intensities can even perform better, which is promising for the ELI-ALPS experiments
- **Two-sided** shooting is **necessary** both for controlled acceleration and simultaneous volume ignition
- Further investigations will go to map the best possibilities of target fabrication

Conclusions, Looking forward

Proton emmision from resonant targets

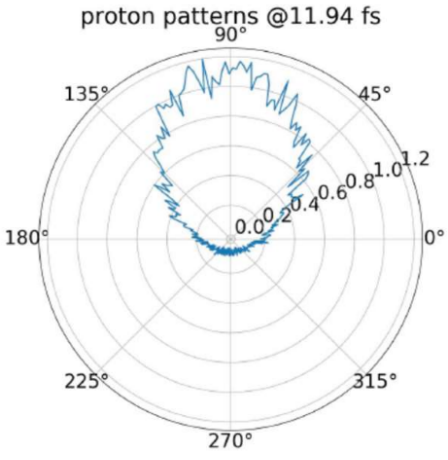

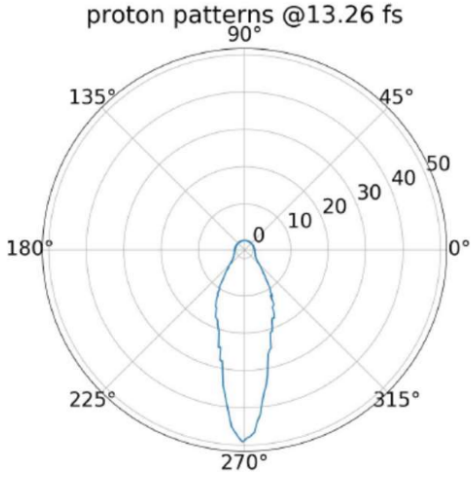

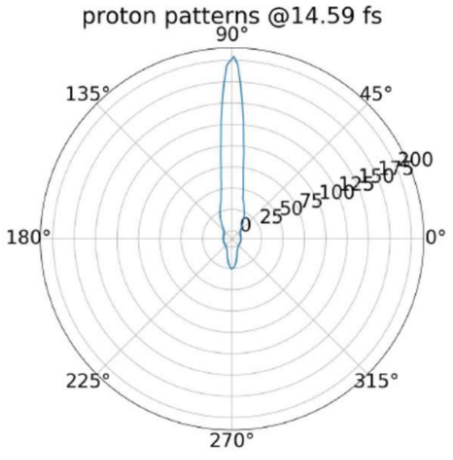

[Nuclear physics method to detect size, timespan and flow in nanoplasmonic fusion L.P. Csernai, T. Csörgő, I. Papp, M. Csete, András Szenes, Dávid Vass, T.S. Biró, N. Kroó; arXiv:2309.05156v3]

Conclusions, Looking forward

Conical rods

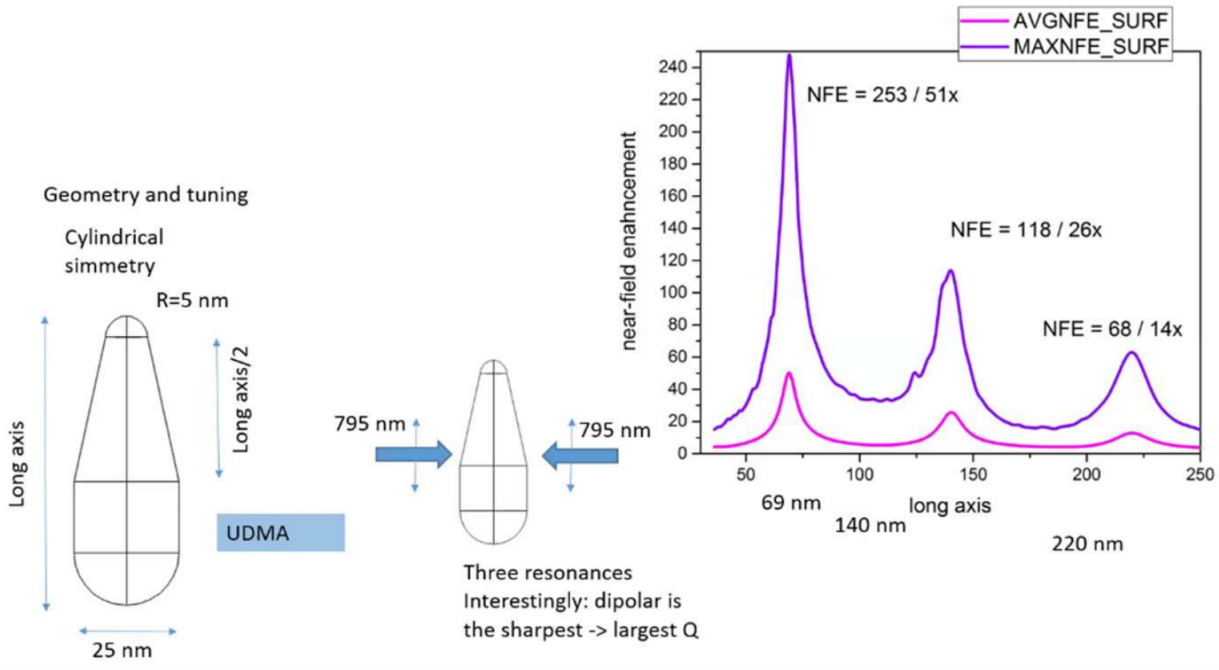

Expectation: **protons** can leave the asymmetric nano-rod antenna more at the **sharp edge** (like in case of lightening rods)

[J. Budai, Zs. Márton, M. Csete, 2024]

Acknoledgements

Enlightening discussions with Prof. Johann Rafelski are gratefully acknowledged. Horst Stöcker acknowledges the Judah M. Eisenberg Professor Laureatus chair at Fachbereich Physik of Goethe Universität Frankfurt. We would like to thank the Wigner GPU Laboratory at the Wigner Research Center for Physics for providing support in computational resources. This work is supported in part by the Frankfurt Institute for Advanced Studies, Germany, the Eötvös Loránd Research Network of Hungary, the Research Council of Norway, grant no. 255253, and the National Research, Development and Innovation Office of Hungary, via the projects: Nanoplasmonic Laser Inertial Fusion Research Laboratory (NKFIH-468-3/2021), Optimized nanoplasmonics (K116362), and Ultrafast physical processes in atoms, molecules, nanostructures and biological systems (EFOP-3.6.2-16-2017-00005). LP acknowledges support from Wigner RCP, Budapest (2022-2.2.1-NL-2022-00002).

We also greatly acknowledge your attention!